EXCITATION AND VAPORIZATION IN ALUMINUM AND URANIUM SUBJECTED TO HIGH PRESSURE SHOCKS

Robert A. Fluegge

Calspan Corporation

Prepared for:

Rome Air Development Center
Advanced Research Projects Agency

January 1975

EXCITATION AND VAPORIZATION IN ALUMINUM AND URANIUM SUBJECTED TO HIGH PRESSURE SHOCKS

Robert A. Fluegge

Contractor: Calspan Corporation
Contract Number: F30602-73-C-0157
Effective Date of Contract: 1 May 1973
Contract Expiration Date: 30 August 1974
Amount of Contract: $79,978.00
Program Code Number: 3E20
Period Covered: August 1973 - September 1974

Principal Investigator: Mr. Robert A. Fluegge
Phone : 716-632-7500

Project Engineer: Mr. Joseph J. Simons
Phone : 315 330-3055

This research was supported by the Defense Advanced Research Projects Agency of the Department of Defense and was monitored by Mr. Joseph J. Simons, RADC (OCSE), GAFB NY 13441 under Contract F30602-73-C-0157.

PREFACE

This research program performed at the Calspan Corporation was supported under ARPA Order Number 1649, Contract F30602-73-C-0157 and was monitored by Joseph J. Simons, RADC (OCSE), GAFB, New York 13441. The contract became effective 1 May 1973 and expired 30 April 1974.

The author would like to thank Mr. W. A. Bullerdiek, Dr. W. J. Rae, Mr. J. Huber and Mr. R. Cooley for their help and many useful discussions during the course of this program.

This report has been reviewed by the RADC Information Office (OI), and is releasable to the National Technical Information Service (NTIS). At NTIS it will be releasable to the general public, including foreign nations.

This report has been reviewed and is approved for publication.

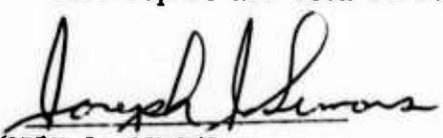

JOSEPH J. SIMONS
RADC Project Engineer

TABLE OF CONTENTS

LIST OF FIGURES

UNCLASSIFIED

SECURITY CLASSIFICATION OF THIS PAGE *(When Data Entered)*

REPORT DOCUMENTATION PAGE	READ INSTRUCTIONS BEFORE COMPLETING FORM
1. REPORT NUMBER: RADC-TR-75-7	2. GOVT ACCESSION NO.
3. RECIPIENT'S CATALOG NUMBER: AD/A-004868	
4. TITLE *(and Subtitle)*: EXCITATION AND VAPORIZATION IN ALUMINUM AND URANIUM SUBJECTED TO HIGH PRESSURE SHOCKS	5. TYPE OF REPORT & PERIOD COVERED: Final - 1 May 73 - 30 August 74
	6. PERFORMING ORG. REPORT NUMBER: WB-5320-A-1
7. AUTHOR(s): Robert A. Fluegge	8. CONTRACT OR GRANT NUMBER(s): F30602-73-C-0157
9. PERFORMING ORGANIZATION NAME AND ADDRESS: Calspan Corporation, P. O. Box 235, Buffalo, New York 14221	10. PROGRAM ELEMENT, PROJECT, TASK AREA & WORK UNIT NUMBERS: 62301D, 16490209
11. CONTROLLING OFFICE NAME AND ADDRESS: Advanced Research Projects Agency, Washington DC 20301	12. REPORT DATE: January 1975
	13. NUMBER OF PAGES: 54
14. MONITORING AGENCY NAME & ADDRESS *(if different from Controlling Office)*: Rome Air Development Center (OCSE), ATTN: Mr. Joseph J. Simons, Griffiss Air Force Base, New York 13441	15. SECURITY CLASS. *(of this report)*: Unclassified
	15a. DECLASSIFICATION/DOWNGRADING SCHEDULE: N/A

16. DISTRIBUTION STATEMENT *(of this Report)*

Approved for Public Release. Distribution unlimited.

17. DISTRIBUTION STATEMENT *(of the abstract entered in Block 20, if different from Report)*

Same

16. SUPPLEMENTARY NOTES

None

19. KEY WORDS *(Continue on reverse side if necessary and identify by block number)*

Shock Heating
Metal Vaporization
Aluminum
Uranium

20. ABSTRACT *(Continue on reverse side if necessary and identify by block number)*

Both uranium and aluminum were shock heated and subsequently allowed to expand into a large, high altitude test chamber. No free uranium atoms were observed. Electronically excited aluminum was seen at real times that corresponded to values which are 10^4 times longer than the known radiative lifetime of the states involved. This means that sizeable numbers of free aluminum atoms are created using shock heating techniques, and further that many of these same atoms are formed in a metastable state or states which lie several electron

DD FORM 1 JAN 73 1473 EDITION OF 1 NOV 65 IS OBSOLETE

UNCLASSIFIED PRICES SUBJECT TO CHANGE

SECURITY CLASSIFICATION OF THIS PAGE *(When Data Entered)*

20.

volts above the ground state. The effects of this metastable on the reaction chemistry are considered; electronically and vibrationally excited AlO can readily be formed if the postulated atomic metastable atom is the ^4P state in aluminum. This finding may help explain some of the variances in the observed chemistry occurring during atmospheric release.

1.0 INTRODUCTION

Techniques for efficient transfer of energy stored in high energy explosives to pure aluminum and uranium discs were studied. The high energy densities available in many commercial explosives make them prime candidates for supplying energy which can be used to vaporize metals, especially when weight considerations are important. This work is an extension of earlier efforts at the Calspan Corporation[1] which produced high vaporization of porous iron when it is processed by similar explosive-generated shock waves.

To study vaporization processes, both uranium and aluminum were formed into targets and impacted by high velocity tantalum flyer plates. The degree of target material vaporized was measured using absorption spectroscopy techniques coupled with high speed recording oscilloscopes. Signals were recorded in real time and their interrelationships used to interpret the sequence of events controlling each experiment. The experimental procedures were closely related to those reported earlier[1] and to those reported by Michel et al[2,3] at the Max-Planck Institute, Germany.

The techniques used in the experimental phases of this program are presented in Sections 2 and 3, and our theoretical approach is outlined in Section 4. Summaries of the experimental results for shock heated uranium and aluminum are presented in Sections 5 and 6, respectively. Section 7 is a summary of the program and the most significant findings presented.

Shock heated uranium was studied in an attempt to find measurable vaporization. Even though an extensive theoretical investigation, based on the work of R.J. Naumann, predicts major vaporization should occur, none was found. Aluminum, on the other hand, is easily vaporized using these same facilities and techniques. Further work is required in the aluminum system since absorption experiments were impossible due to dominant radiation being found at both 3944.01Å and 3961.51Å (allowed transitions to the ground state in Al I). An analysis is presented which tentatively explains the observed irradiance in terms of a postulated metastable state in the Al I system. The state is not identified here; however, its effective lifetime is estimated. Consequences of this metastable state on the effective chemistry of aluminum reacting with atmospheric gases is then considered.

2.0 EXPERIMENTAL APPROACH

The experimental facilities used to verify the shock heating techniques incorporated into this program have been described elsewhere,[1] and as such only a brief outline of the system will be given. The overall program goal was to obtain significant vaporization in both uranium and aluminum. The Calspan high altitude test chamber shown in Figure 1 was used to enable low pressure operation and to contain these experiments. Pressures as low as 10^{-6} torr were readily attained as the program progressed. Lower pressures produce data which is more easily interpreted since collisional effects with background gases and subsequent line broadening effects are minimized.

A flyer plate launch assembly is located at the right hand end of the 12.2 meter long chamber shown in Figure 1. It contains high energy explosives for driving the flyer plate. The launch assembly placement is critical since a known distance between it and the 1000 watt Xe-arc lamp is required for velocity determinations. The Xe arc lamp has an intense continuum applicable for absorption measurements at wavelengths near 3800 to 3900 Å. A 1/2-meter Jarrell-ash monochrometer was modified to incorporate three photomultiplier detectors in its exit plane; it was used to record the output of the continuum light source as shown. These signals change as light absorption and/or scattering occurs within the chamber between the light source and the detectors. The reduced signal intensities can be interpreted as being due to either resonant absorption at an allowed transition of the atom under study or due to continuum absorption by particulates and/or molecular species present. Absorption lines at 3871.04 Å and 3943.82 Å were used in uranium; similarly, the 3944.01 Å and 3961.54 Å lines were centered in the Jarrell-ash monochrometer for the Al I system.

Intensity calibrations were performed and the output signals related to irradiancies measured using an EG&G Model 580 radiometer coupled to a narrow-band interference filter. Exact wavelength determinations were made using several cold cathode discharge lamps; Fe, Al, and U having emissions which were of main interest here. Daily realignment and calibration was required due to the high resolution ($\pm$ 1.5 Å) requirements in these experiments. The detection system was found to be quite stable over many hours after an initial 1-1/2 hour warmup period.

The experiments with aluminum started out using normal absorption procedures. However, as will be explained in more detail in Section 6, the light flux emerging from the test volume exceeded input values from the continuum lamp. This was only true at resonant wavelengths in aluminum; hence, a long-lived metastable has been postulated. Since procedures in an emission experiment require irradiance determinations to find the number of radiators in the test chamber, absolute calibrations were incorporated.

A high speed image converter, TRW Model #1D, was used to make measurements of the axial and radial velocities within the expanding jet, produced by detonating the flyer plate launch assembly. At a preset time after detonation, an EG&G flash lamp, located as shown in Figure 1, is triggered and generates a light beam of about 50 million candle power. It has a 1.5 μsec duration time. A shadow is produced on a translucent, Mylar screen located within the test chamber; the shadow is caused by light absorption and scattering. Knowing the exact time at which detonation occurred, and the time at which the shadowgraph was taken, enables calculation of the radial and axial velocity components.

Pressures within the test facility were measured using both an MKS Baration and a Veeco Ionization gauge. Each correlated with the other within a factor of 2 in their ranges of overlap. Total light intensity in the chamber was determined using high speed photodiodes. Their outputs were recorded, along with all other parametric measurements, on high speed oscilloscopes.

2.1 Flyer Plate Launch Assembly

The heart of the flyer plate launch assembly is a 30 gm main charge pellet shown in Figure 2. It is commercially designated as PBX 9404 and is composed of 94% HMX with a 6% binder consisting of equal parts nitrocellulose and tris-β-chloro-ethyphosphate. Detonation velocities near 8.8 km/sec at the 1.84 g/cc used here have been measured.[4] PBX 9404 has been used extensively as a metal accelerator by previous experimentalists[5] and was picked for use here based on previous experience, both at Calspan and elsewhere.

A twelve-point distributor plate was incorporated, as shown in Figure 2, to translate a single input detonation to twelve simultaneous outputs. It is fabricated of Lexan polycarbonate plastic and extrusion loaded with Extex 8003, an 80% PETH-20% silicone elastomer bonded explosive. Test fire results indicate that the average transit time from input to output is 2.54 μsec with a standard deviation from point to point of 0.04 μseconds. Thus, a plane wave is generated which can uniformly spread into the PBX 9407 booster pellet.

The PBX 9407 booster pellet is composed of 94% RDX bonded with 6% Exon 461 plastic and has a steady state detonation velocity of 7.9 km/sec. It provides a smooth transition of the detonation from the distributor plate to the main charge.

Tantalum flyer plates were used throughout these experiments; two thicknesses were used, 0.005"and 0.010" by 1.2" diameter. The 0.005" thick flyer plate could be accelerated to 9 km/sec which is near the detonation velocity of the PBX 9404 main charge. This particularly high flyer plate velocity was accomplished using the confinement techniques described below.

2.2 Detonation Confinement Chamber

A steel holder was designed and incorporated in these experiments to increase the coupling efficiency between the main H.E. charge and the flyer plate. Figure 3 shows this assembly coupled to the uranium target shield and holder. The flyer plate launch assembly is packed into the steel holder and the backplate held in place by eight steel bolts. A small hole is machined into this plate to enable the detonator holder and detonator to protrude beyond the right hand end.

Uranium targets were cemented onto their copper (or aluminum) holder as shown. The opposite end of this holder is sealed using a polyacetate film attached to the tantalum flyer plate. A removable, brass cover plate, coupled with an o-ring seal, is used to seal the left hand end of the holder. As a

result, the uranium target and tantalum flyer plate can both be held in an inert atmosphere during pumpdown procedures performed on the high altitude test chamber.

A flexible hose is attached to this holder which is connected to control valves located at the chamber walls. The valves are controlled so as to maintain pressures internal to the target holder assembly equal to those measured in the high altitude test chamber. The brass cover plate is removed from the assembly by external cabling after pumpdown and just before final checkout and detonation procedures.

The extreme care exercised in these experiments to protect the uranium targets was incorporated to reduce the possibility of oxides forming on the uranium surfaces. Targets made of pure aluminum were used in the second half of these experiments; they did not require the extreme care and procedures as that used for uranium.

Flyer plate velocities were determined using piezoelectric pins manufactured by EG&G Inc., placed as shown in Figure 3. The signals produced by these pins, as impact occurs at their surface, were monitored on high speed oscilloscopes. The time difference and premeasured separation between the front surfaces were used to calculate flyer plate velocities. All measurements fell within the readability on the oscilloscope face, $\pm$ 5%. Piezoelectric pins were employed here since they are not subject to preionization effects, as was the case for the electrical shorting type pins used on previous programs.

3.0 VAPORIZATION

The number of atoms that are released as a result of shock heating was determined by atomic absorption spectroscopy. Since the expected concentrations were high, line shapes are dominated by pressure broadening; a computer program was used to calculate their shapes. Absorption was determined by integrating over calculated line shapes and the transmitted light flux compared to measured signals. The comparison enables direct determination of the free atom densities in the high altitude test chamber at any predetermined time. The approach requires most atoms to be in their ground state. However in the case of aluminum, these techniques were inapplicable since resonant radiation was measured which exceeded the input photon flux.

The flow field contains solid, liquid, and gaseous particles. Personnel at the Lawrence Livermore Laboratory[6] have performed some in vacuo detonation product studies with HMX. Examination of their unpublished data indicates good agreement with theoretical analysis with the exception of solid carbon. T. K. Mehrhoff of the Burlington AEC Plant, has run combustion studies in air with PBX 9404.[7] His results show a great deal of ash formation, presumably containing substantial quantities of free carbon. Performing these tests in air causes an enhancement of CO_2 and NO_x as might be expected. Table 1 is a list of gases and solids that would be released by a detonation; it is based on theoretical decomposition considerations, the Lawrence Livermore Laboratory data, and the Burlington work. All products, including binder materials, from the detonated flyer plate launch assembly have been included.

It should be noted that these estimates are at equilibrium conditions. A number of atomic and molecular species are undoubtedly present in various degrees of excitation immediately following detonation.

TABLE 1

Quantitative Estimates of Expected Decomposition Products
From the Calspan Type Flyer Plate Launch Assembly

Gases	Solids	Test Materials
N_2 - 8.3 liters at S.T.P.	C - 0.84 gm	Tantalum Flyer
H_2O - 7.1 liters at S.T.P.	P_2O_5 - Trace	Uranium Target
CO_2 - 4.2 liters at S.T.P.	SiO_x - Trace	
CO - 2.2 liters at S.T.P.		
NH_4 - 0.9 liters at S.T.P.		
H_2 - 0.7 liters at S.T.P.		
NO_x - 0.4 liters at S.T.P.		
HCN - Trace		
HCl - Trace		
HF - Trace		

To distinguish between the number of free atoms and other materials present, the absorption in three wavelength regions was measured and compared. For example, the gas phase absorption by uranium was monitored at 3871.04 $\pm$ 1.5 Å which corresponds to the transition between the $^5L_6$ ground state and an allowed upper state. The measured oscillator strength for this line is reported by NBS[8] to be 0.0923. Scattered light was monitored at 3859 $\pm$10 Å and 3883 $\pm$10 Å to bracket the resonant uranium absorption line. The signal differences between continuum and resonant absorption were used to determine the number of atoms in the light path. The following is an outline of the calculation procedures applied to these absorption measurements.

The number of atoms, dn, in a symmetric jet of radius Y_B and of length dx at a given time is given by:

$$\frac{dn}{dx} = \int_0^{Y_B} \rho 2\pi y dy \qquad (1)$$

where: ρ = atom density.

The atom and particulate velocities are assumed equal, constant in time, and originating from a point source at time, t. Thus, flow velocities are given by

$$\dot{X} = \frac{X}{t} \quad \text{and} \quad \dot{Y} = \frac{Y}{t} \tag{2}$$

where: Y = radial dimension of the expanding jet
X = axial dimension of the expanding jet

and the gas density distribution can be described by[3,9]

$$\rho = \rho_t \cos^m \left(\frac{\pi}{2} \frac{Y}{Y_B}\right) \tag{3}$$

where: ρ_t = symmetric jet centerline density
m = constant; taken to be 2 based on previous experience.

Substituting equation (3) into (1) gives

$$\frac{d\eta}{dx} = 2\pi\rho_t \int_0^{Y_B} y \cos^2 \left(\frac{\pi}{2} \frac{y}{Y_B}\right) dy \tag{4}$$

The differential light transmission due to the atomic and particulate matter is given by

$$\frac{dI}{d\lambda} = \exp \{-2 \Sigma_i \int_0^{y'} k_i dy\} \tag{5}$$

where: y' = minimum of Y_B and 198.12 cm (the inside radius of the Calspan test facility)
k_i = absorption coefficient due to either atoms, molecules, or particulates

For atomic species, the absorption coefficient is given by

$$k_a = \frac{e^2 \lambda^4 f}{4\pi m_e C^3} \left(\frac{\gamma_N + \gamma_C}{(\lambda - \lambda_C)^2}\right)^2 \rho \tag{6}$$

where: $e = 4.8032 \times 10^{-10}$ esu

$c = 2.9979 \times 10^{10}$ cm/sec

$m_e = 9.1055 \times 10^{-20}$ gm

$\gamma_N = f g_m / 1.499 \ \lambda_c^2 \ g_n$

$\gamma_C = 1.92 \sqrt{\frac{g_m}{g_n}} \frac{e^2}{me} \frac{\lambda}{c} f\rho$

$\lambda_C = 3871.04$ Å for uranium

$f = 0.0923$ for uranium

$g_m = g_n = 13$

Substituting equation (6) into (5) and integrating over the pathlength, Y_B, gives optical transmission as a function of wavelength and number of atoms per unit axial length (dn/dx). The calculations at various centerline densities and values of dn/dx can be used to relate measured transmissions to corresponding values of dn/dx. A plot of such curves is shown in Figure 4. Transmission is given for values of dn/dx as a function of the radial expansion parameter, Y_B. Each experimental transmission measurement at 3871.04 Å can then be used to determine a value for the number of uranium atoms in the expanding jet.

The monochrometer exit-plane detector configuration, which was used to compare continuum with resonant absorption, is shown in Figure 5. Microscope cover slides were aluminized and placed so as to divide the photon flux from the Jarrell-Ash monochrometer into three photodetectors. Dumont type 6467 photomultiplier tubes were placed so as to detect the resonant absorption line (photomultiplier #2), the continuum absorption over the adjacent 20 Å toward the ultraviolet (photomultiplier #1) and the continuum absorption over the adjacent 20 Å toward the red (photomultiplier #3). Prior to each experiment, a hollow cathode discharge lamp was used to adjust the center slit so as to have the 3871.04 Å resonant line exactly in the middle of the center exit slit. Each photodetector output was fed to recording oscilloscopes. Comparing the three recorded signals at known times enables a direct determination of preferential absorption due to free atoms and as well the velocity of the expanding jet relative to the particulates and the other explosively released products.

3.1 Expanding Jet - Velocity Measurements

A series of shadowgraphs were taken to obtain a relationship between the radial and axial velocities in the expanding jet. The photographic system included a TRW Model 1D Image Converter Camera in combination and a high power flashlamp. The flash duration was set at 1.5 microseconds. The open time of the TRW image converter was 10^{-8} seconds. A satisfactory combination of light intensity and shadow definition was extremely difficult. As a result, shadowgraphs showing the jet were not sufficiently clear for use.

Since a relationship between the axial and radial velocities is required to analyze the data, the velocity profiles from similar investigations were used. Figure 6 was obtained from data published by Michel et al.[9] The radial velocity, $\dot{Y}$, is shown as a function of the axial velocity, $\dot{X}$. The two curves show the differences between a plane wave ($2\alpha = 180^{\circ}$) system and a shaped charge ($2\alpha = 45^{\circ}$) configuration. The velocity distribution for the latter (Figure 6b) was used to analyze the data presented in this report. The majority of our experiments were conducted using the metal confining techniques (see Figure 3) and hence, the velocity distribution from a shaped charge system appears to best represent the system used here.

4.0 THEORETICAL PREDICTIONS

Researchers have applied various equations of state to find reasonable correlations between predicted and measured thermodynamic parameters. One such equation-of-state, proposed by R. J. Naumann[10,11], has been successfully used in several studies of metals subjected to high pressures and temperatures. As a result, Naumann's analytical approach to describe increases in system entropy, pressure, and temperature was incorporated.

Impedance matching techniques for a tantalum flyer plate impacting on uranium targets were applied and used to determine the data presented in Figure 7. The Hugoniot curves for normal density uranium and tantalum were taken from the data compiled by M. van Thiel, et al[12] (at Lawrence Radiation Laboratory) and interpolated using Naumann's equation-of-state. The curve-crossing points in the figure represent expected particle velocities in the target; the value attained is highly dependent upon the target porosity. Once the target particle velocity and corresponding post shock pressures are known, the analysis to determine other themodynamic parameters can proceed.

Substituting Naumann's equation-of-state for uranium into the Hugoniot relation,

$$\xi_1 (p_1 V_1) - \xi_o (p_o V_o) = \frac{1}{2} (p_1 + p_o) (V_o - V_1) \qquad (7)$$

where ξ = internal energy
V = volume
P = pressure
subscript "o" is the pre-shocked condition
subscript "1" is the post-shocked condition

allows direct calculation of the thermodynamic variables of the post-shocked material. Figure 8 is an example of the results obtained from computer calculations. For a given post-shock pressure, the post-shock specific volume can be determined. The curves presented in the figure represent this relationship for various porosities in uranium. The more porous the target, the higher the post-shock pressure for a given relative volume, V/V_o.

This equation-of-state can be applied to calculate the entropy increase in target material at a given particle velocity. Typical results are presented in Figure 9. The more porous target materials (larger values of m) produce greater values of entropy at a given particle velocity. For example, consider the Calspan flyer plate launch assembly which accelerates a Ta flyer plate to 9 km/sec. Tantalum flyer plates traveling at this speed and impacting on porous uranium targets produce major particle velocity increases. The impedance matching techniques presented in Figure 7 predict a particle velocity increase in uranium of 5.5 km/sec for a distention ratio of 2. The post shock pressure is 4.5 mb. As a result, the targets relative volume would have decreased to 0.7 of its initial values as shown in Figure 8, and its entropy would have increased to 58 cal/mole-°K as indicated in Figure 9. The approach used here is to assume that isentropic unloading occurs in the target as it expands into the vacuum of the high altitude test chamber. The shock heating process used in these experiments should produce liquid uranium droplets having an entropy of 58 cal/mole-°K; moving at high velocities down the chamber's axis. This hot liquid should vaporize causing a corresponding decrease in droplet temperature and release free uranium atoms. An entropy of 58 cal/mole-°K in uranium predicts a temperature sufficient to cause major vaporization. To see this, the data presented in Figure 10 shows that an entropy increase to 58 cal/mole-°K produces a state change and corresponding temperature which is well above the boiling point at atmospheric pressure. The result should be nearly total vaporization.

5.0 SHOCK HEATED URANIUM

Discs having porousities covering the range between 47% and 85% of normal crystalline densities were shock heated. The degree of vaporization produced by this heating procedure was measured for tantalum flyer plates impacting on uranium targets. The uranium matrix in the pre-shocked condition was studied using both optical and electron microscopy. D. E. Lozier and W. H. Pfiefer of Battelle-Columbus Laboratories were instrumental in the uranium target preparations and initial handling; their final report covering these sample preparations is included as Appendix A to this report. Similar purity and morphology verification tests were performed at Calspan Corporation using an ETC scanning electron microscope. The Calspan results, shown in Figure 11, substantiate the Battelle findings. One major problem not addressed by these investigations is the possible surface oxidation on the sample. It may well be that this oxidation is an inherent difficulty in studying vaporization processes in uranium.

Normalized monochrometer signals, as measured for one of the eleven experiments completed on porous uranium, are presented in Figure 12. The curve labeled resonant absorption was recorded to determine the relative absorption at 3871.04 $\pm$ 1.5 Å, an allowed transition in the UI system. As a comparison, one of the two sideband radiometer recordings is also shown in the Figure. The noise evidenced here (and on all similar tests in uranium) indicates that little or no vaporization occurs. At least several percent of the initial target plate would have to vaporize to produce measurable signals. The lack of substantial vaporization is consistent with the recent findings of M.P.I.; they find no more than 1% vaporization occurs in their uranium studies.[2] However, the much higher flyer plate velocities with accompanying increases in target entropy and temperature estimated in these experiments should have produced substantial vaporization. No clear explanation is available; further experimentation and procedure verification are required.

6.0 SHOCK HEATED ALUMINUM

A series of experiments, similar to those conducted in uranium, were performed to study shock heating processes in aluminum. Initial experiments to obtain absorption signals in ground-state atoms were thwarted since an irradiance increase was measured rather than the normal decreases experienced in other atomic systems. Typical signals are presented in Figure 13. The upper trace shows resonant signals at 3944.01 ±1.5Å, and the lower trace indicates continum radiation levels (as measured using a photo-diode) within the Calspan high altitude test chamber due to the energetics of the detonation.

Several experiments to investigate these anomalous emissions in the Al I system were performed. As has been noted above, the output signals from the Jarrell-ash Monochrometer, located as shown in Figure 1, were seen to increase in intensity over the incident continuum Xe-arc lamp radiation. These measured increases were measured at both 3944.01 Å and 3961.53 Å. The measured increases were in a ratio of about 2 to 1, consistent with the lower state's multiplicities. As an aid in discussing emissions in the Al I system, an energy level diagram[14,15] in aluminum is given in Figure 14. The two atomic emissions observed originate in the 4s $^2S_{1/2}$ state; the lower atomic state is either the $^2P_{1/2}$ (for the 3944.01 Å) for the $^2P_{3/2}$ (for the 3961.53 Å). However, the total lifetime of the 4s $^2S_{1/2}$ state is only 7×10^{-9} seconds, and the emissions observed here occur at times between 0.5 and 1.0×10^{-3} seconds after formation. As a result, a longer lived metastable state seems to be a factor in controlling the observed emissions.

A quartet state that could function as a metastable in the Al I system, ^4P, is shown at the right of the energy level diagram. For this state to be contributing to the observed radiation, an interconnecting transitions must exist to the 4s $^2S_{1/2}$ state. However, time limitations, precluded any attempts to verify this point during these experiments. The ^4P state, interestingly, has been observed to couple to autoionizing states, such as the ^4D state shown in Figure 14. There may exist a high probability for forming this highly excited neutral species due to electron-ion recombination with subsequent radiative decay to the ^4P state. The mechanisms and various routes available for this atomic relaxation remain to be determined.

Figure 15 indicates the observed time relationship between the anomolous emissions seen at 3944.01 $\pm$ 1.5 Å and two related radiometer measurements taken during the same experiment. The two sideband radiometers monitor emissions over 20 Å bandwidths shorter than 3942 Å and longer than 3946 Å, respectively. The peak in the narrow band radiometer (λ_c = 3944.01 Å) occurs 0.5 milliseconds after the flyer plate launch assembly explosion and the Ta flyer plate impact on the pure (99.98%) aluminum target. The flyer plate takes only 5×10^{-6} seconds to travel from its launch point to the aluminum target due to the highly efficient coupling with the H.E. and subsequent high velocities encountered. Hence, impact is indicated as occurring essentially simultaneously with detonation due to the time scale in the figure. The two sideband radiometers show small increases in this same time period which may be a result of light leakage between the radiometers and/or natural line broadening at higher atomic densities. A photodiode output which is proportional to the continuum emissions in the explosive fireball is also shown in Figure 15. This photodiode was located on the side wall of the high altitude test facility and pointed directly at the flyer plate launch assembly. Comparing time relationships between these four signals enables a direct comparison of their origins.

The emissions that are a result of the explosive ignition represent a continuum which contributes little, if any, to the three narrow band radiometer signals. This is evident by comparing signal amplitudes at corresponding real times. The peak of the continuum photodiode occurs at 0.2 ms after explosive ignition and returns to 10% of its peak value by 0.6 ms. No comparable peak signals occur in the three narrowband radiometer signals. On the other hand, the marked increase seen at 3944.01 Å does not contribute significantly to the continuum radiation. As a result, the two signals seem to be independent and to have separate origins.

The irradiance at the Jarrell-ash radiometer entrance slit was calibrated using an EG&G Inc., Model 580 radiometer coupled with a narrow band interference filter. A continuum light source was used in these calibration procedures. Curve multiplying techniques were applied to the calibrated detector values coupled with the known filter transmission curve. The

measurements were then compared and used to normalize the narrowband radiometer signals, which recorded the irradiance at resonant wavelengths in the Al I system.

The spectrometer entrance slit was located at the focal point of a lens located near the high altitude test chamber wall (see Figure 1). The slit adjusted (0.15 mm x 0.2 mm) to ensure high resolution ($\pm$1.5 Å) at the photomultiplier detector. As a result, this is the limiting optical element and its acceptance solid angle, Ω, is given by

$$\Omega = A_s/f^2 \tag{8}$$

where: A_s = entrance slit area, 0.03 mm^2
f = lens focal length, 330 mm

Within the accuracy required here, the effective solid angle seen by each contributing volume within the high altitude test chamber is constant and equal to Ω. This can be seen by envisioning a cylinder, bounded at one end by the detector lens assembly and on the other end by the high altitude test chamber walls. Its radius is determined by the detector lens assembly. Excited atoms that pass through and radiate within this cylinder contribute to the detected signals. The irradiance at the spectrometer entrance slit is given by:

$$I = \int_{-Y_B}^{+Y_B} \frac{1}{4} A_{mn}^2 \, r^2 \Omega \frac{hc}{\lambda_c} \rho_c \, \mathrm{Cos}^2 \left(\frac{\pi}{2} \frac{y}{y_B}\right) dy \tag{9}$$

where: A_{mn} = transition probability from the 4s $^2S_{1/2}$ to the $^2P_{1/2}$ states, 0.47 x 10^8 sec^{-1}
h = 6.6253 x 10^{-27} erg-sec
c = 2.9979 x 10^{10} cm/sec
λ_c = 3944.01 x 10^{-8} cm
r = radius of sensitive cylinder, 3.8 cm
Y_B = radius of symmetric jet of excited atoms, cm

Ω = solid angle, A_s/f^2

ρ_c = density of excited atoms in the high altitude test chamber centerline, atoms/cm^3

Integrating equation (9) with respect to γ and inserting the defined constants gives

$$I = 2.4 \times 10^{-9} \rho_c Y_B \text{ ergs/sec cm}^2 \quad (10)$$

This relationship will be used to determine the extremes available to the postulated metastable's lifetime.

6.1 Metastable States Which Control the Al I Emissions

Limits on the lifetime of the metastable state and/or states which control the anomolous radiation seen in Al I can be estimated using rate equation analyses. For example, define an effective metastable state, A_1, of the atom (such as the ^4P) which spontaneously decays to the 4s $^2S_{1/2}$ state of aluminum. (See Figure 14 for an energy level diagram.) The 4s $^2S_{1/2}$ state decays in 7×10^{-9} seconds to either the 3 p $^2P_{1/2}$ or the 3 p $^2P_{3/2}$ ground state configuration through the emission of a photon, which has a wavelength of 3944 Å or 3961.5 Å, respectively. The decay scheme can be represented by

$$[A_1] \xrightarrow{\tau_1} [A_2] + h\nu_1 \quad (11)$$

$$[A_2] \xrightarrow{\tau_2} [A_G]_{1/2} + h\nu_2 \quad (12)$$

$$[A_2] \xrightarrow{\tau_3} [A_G]_{3/2} + h\nu_3 \quad (13)$$

where: $[A_1]$ = the number of unknown metastable atoms in aluminum

$[A_2]$ = the number of atoms in the 4s $^2S_{1/2}$ state

$[A_G]_{1/2}$ = the number of atoms in the $^2P_{1/2}$ state

$[A_G]_{3/2}$ = the number of atoms in the $^2P_{3/2}$ state

τ_1 = lifetime of the unknown metastable

$(\tau_T)^{-1}$ = total transition probability, 1.4×10^8 sec^{-1}

$(\tau_T)^{-1} = (\tau_2)^{-1} + (\tau_3)^{-1}$

Equations controlling this decay scheme are

$$\frac{d\,[A_1]}{dt} = -\frac{1}{\tau_1}\,[A_1] \tag{14}$$

and

$$\frac{d\,[A_2]}{dt} = \frac{1}{\tau_1}\,[A_1] - \frac{1}{\tau_T}\,[A_2] \tag{15}$$

These two differential equations can be solved to obtain

$$[A_1] = [A_1]_0 \exp\,(-t/\tau_1) \tag{16}$$

and

$$[A_2] = [A_2]_o + \frac{\tau_T\,[A_1]_0}{(\tau_T - \tau_1)} \exp\,(-t/\tau_T) - \frac{\tau_T[A_1]_0}{(\tau_T-\tau_1)} \exp\,(t/\tau_1) \tag{17}$$

where: the subscript "o" represents concentrations at $t = t_o$.

Assuming $\tau_1 >> \tau_T$, as would be the case for a metastable, equation (17) simplifies to

$$[A_2] = \frac{\tau_T}{\tau_1}\,[A_1]_0 \exp\,(-t/\tau_1) \tag{18}$$

As will be seen, the number of atoms in the $[A_2]$ state ($4s\ ^2S_{1/2}$) can be related to the measured irradiance at 3944.01 Å; in addition, τ_T and t are known from the literature and the experimental conditions. Hence, τ_1 and $[A_1]_o$ have a well defined relationship.

6.2 Experimental Results in Aluminum

Emission, rather than absorption, signals were observed in shock heated aluminum. An estimate of the number of excited atoms in the expanding jet at any given instant in time requires finding a correlation function between absolute irradiance of the monitoring radiometer and a known standard, such as the EG&G Model 580 used here. Full scale (1.0) in Figure 15 for the resonant radiometer set at 3944.01 Å corresponds to an irradiance of 0.0418 ergs/cm^2 sec. Substituting the known constants and initial conditions into equation (10) gives

$$\rho_c = I/2.4 \times 10^{-9}\ Y_B, \tag{19}$$

the centerline density at any instant in time.

To determine the extent of the expanding jet at any given time, Y_B is assumed to follow a distribution similar to that found in previous experiments. It is given by

$$Y_B = \dot{y}\, t \tag{20}$$

where: $\dot{y}$ = radial velocity of the vapor - particulate cloud as given in Figure 6.

t = time after flyer plate impact on the aluminum target

To use Figure 6, the axial velocity,

$$\dot{X} = d/t \tag{21}$$

where: d = the distance from the target plate to the monochrometers line of sight, 231 cm

of the cloud must be determined. Thus, the centerline density at any instant in time is calculable. Substituting these velocities into equation (1) and integrating over Y_B enables a point by point determination of dn/dx as a function of x; the results of such a calculation are presented in Figure 16.

The integral of the experimental curve shown in Figure 16 is a direct measure of the number of atoms within the flow stream. This area corresponds to $7 \times 10^{+10}$ radiating atoms within the expanding jet at approximately 0.5 ms after release. Inserting this number of atoms into equation (18) gives

$$[A_1]_0 = 9.85 \times 10^{18} \tau_1 \exp (5.13 \times 10^{-4}/\tau_1) \qquad (22)$$

Figure 17 is a graphical presentation of equation (22). For each initial value of metastable atoms, $[A_1]_0$ there are two lifetimes that satisfy the conditions and measurements taken. Of course, future experiments should include concentration measurements as a function of distance down the expanding jet to unequivocally determine the lifetime of this postulated metastable state. As can be seen in the Figure, τ_1 must be larger than 2×10^{-5} seconds; its magnitude depends on how many metastable atoms were initially formed. It is also evident from the curve that at least 10^{16} (or 1 in 10^7) atoms were initially in this excited state. Further work remains to better define the radiative decay scheme, the upper state or states involved, better measurements of their lifetimes, and the overall effect of these findings on the reaction chemistry in aluminum.

6.3 Reaction Kinetics of Aluminum

Recent experimental and theoretical studies of aluminum chemistry in atmospheric gases assumes that the atom is found in, or quickly relaxes to, its ground electronic state. The possibility of a significant fraction of the reacting atoms being formed in a long-lived electronic state adds several alternate reaction schemes. The postulated ^4P metastable state in aluminum lies about 29,900 cm^{-1} (3.7 ev) above its ground state as shown in Figure 14.

The possibility of this reaction causing an eight-fold increase in the reaction cross section for the Al + O_2 reaction was postulated by Fluegge et al[17] according to Harpoon model predictions. As a result, the following reactions are energetically possible and can produce significant internal excitation:

$$Al(^4P) + O_2(X^3\Sigma_g^-) \longrightarrow \begin{cases} AlO(X^2\Sigma^+) + O(^3P) + 71 \text{ kcal} \\ AlO(X^2\Sigma^+) + O(^1D) + 26 \text{ kcal} \\ AlO(A^2\Sigma^+) + O(^3P) + 32 \text{ kcal} \end{cases} \tag{23}$$

There is sufficient energy to form the $A^2\Sigma^+$ state in AlO and in addition to add to its total vibrational excitation. The net result could be a significant input to the observed radiation from grenade releases into the atmosphere as outlined by Linevsky and Alyea[18]. The total contribution to the reaction chemistry and subsequent radiative relaxation processes can be further studied using the techniques outlined here.

7.0 SUMMARY

Both uranium and aluminum were shock heated and subsequently allowed to expand into a large, high altitude test chamber. No free uranium atoms were observed. Electronically excited aluminum was seen at real times that corresponded to values which are 10^4 times longer than the known radiative lifetime of the states involved. This means that sizeable numbers of free aluminum atoms are created using shock heating techniques, and further that many of these same atoms are formed in a metastable state or states which lie several electron volts above the ground state. The effects of this metastable on the reaction chemistry are considered; electronically and vibrationally excited AlO can readily be formed if the postulated metastable atom is the ^4P state in aluminum. This finding may help explain some of the variances in the observed chemistry occurring during atmospheric releases.

REFERENCES

1. Fluegge, R.A., "Explosive Techniques for High Altitude Metal Releases," Report # RADC-TR-73-307. August 1973.

2. Michel, K.W. and Hornung, K. "Studies on Shock Vaporization of Transition Metals Uranium and Iron", Personal communication in draft form 1973.

3. Hornung, K. and Michel, K. W., J. of Chem. Phys. 56 p. 2072 (1972).

4. Jones, O. E., "Metal Response Under Explosive Loading," Sandia Corporation, presented at the ASME Symposium, University of New Mexico, March 1972.

5. Kury, J. W., et al., "Metal Acceleration by Chemical Explosives," Lawrence Radiation Lab. Proc. of the 4th Symposium on Detonation, ACR-126, Office of Naval Research.

6. Private communication.

7. Private Communication.

8. Corliss, C. H. and Bozman, W. R. Experimental Transition Probabilities for Spectral Lines of Seventy Elements NBS Monograph 53 (1962)

9. Brunner, W., Foppl, H., and Michel, K. W., Astronautica Acta. 15 p. 613 (1970).

10. Naumann, R. J., Ph.D. Thesis, University of Alabama 1970.

11. Naumann, R. J., NASA Report No. TN D-5892, 1970.

12. van Thiel, M., Kusubov, A. S., and Mitchell, A. C. "Compendium of Shock Wave Data" UCRL-50108 Oct. 1967.

13. Hultgren, R., Orr, R. L., Anderson, P. D. and Kelley, K. K., Selected Values of Thermodynamic Properties of Metals and Alloys, Wiley and Sons (1963).

14. Chandler, A. C. Atomic Spectra D. Van Nostrand Co. Inc. 1964.

15. Herzberg, G. Atomic Spectra and Atomic Structure Dover Publications 1944.

16. Naumann, R. J., J. Applied Physics 42 p. 4945 (1971).

17. Fluegge, R. A., Hendrick, R. D., and Landman, D. A. "Project Barium Metastables" RADC-TR-70-262 Nov. 1970.

18. Linevsky, M. J. and Alyea, F. N. "Spectroscopy of Metal Oxides" RADC-TR-73-391 Nov. 1973.

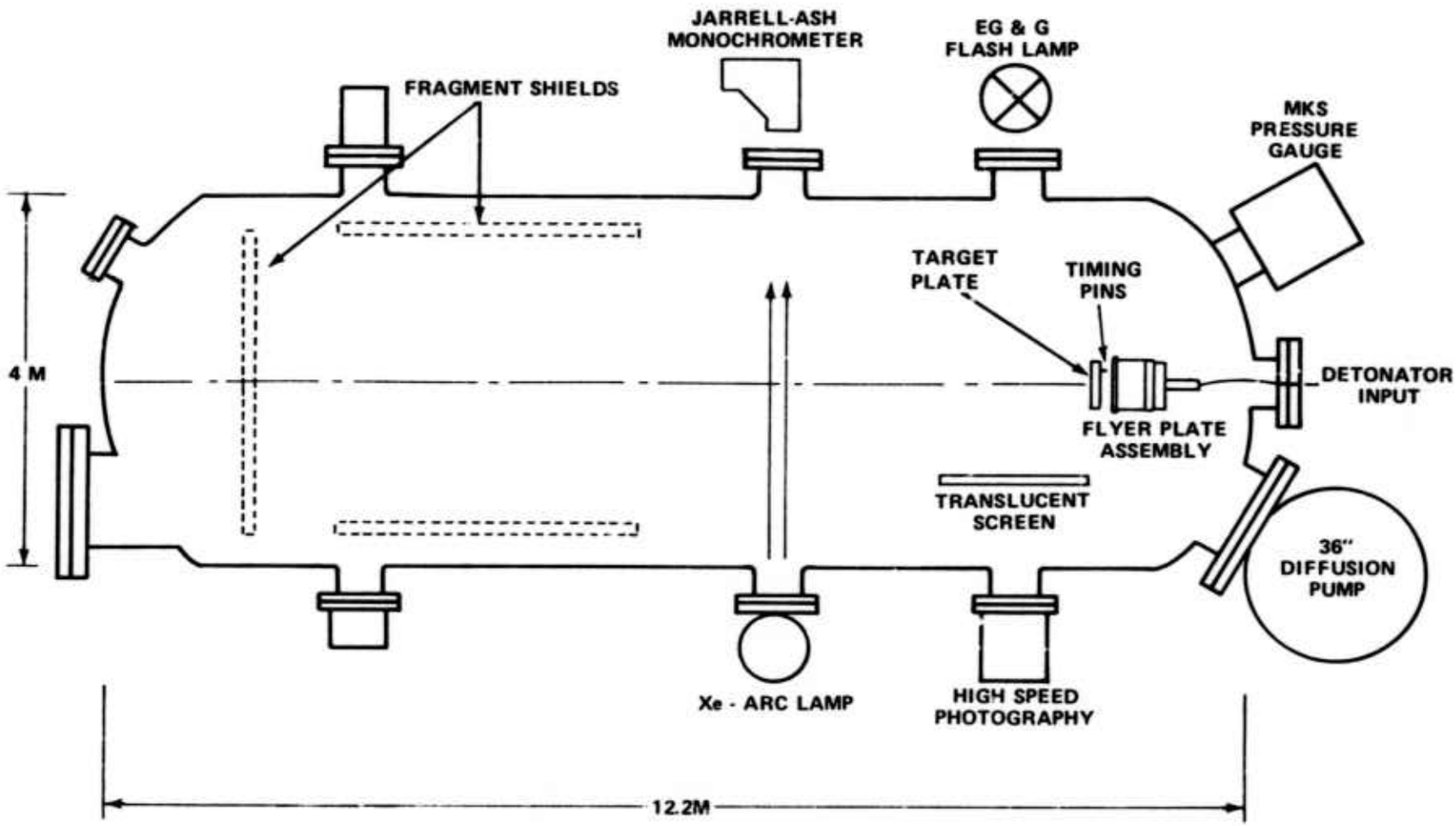

Figure 1 CALSPAN HIGH ALTITUDE METAL RELEASE TEST FACILITY

1. REYNOLDS RP-87 EBW DETONATOR
2. DETONATOR HOLDER
3. DISTRIBUTOR PLATE, EXTRUSION LOADED W/EXTEX 8003 HIGH EXPLOSIVE
4. H.E. BOOSTER PELLET, PBX-9407
5. H.E. MAIN CHARGE W/ALTERNATE EXPLOSIVES
   PBX-9404
   PBXN-5
6. POLYACETATE FILM, 0.003" THICK x 1.2" DIA.
7. TANTALUM FLYER PLATE, 0.005" OR 0.010" x 1.2" DIA.

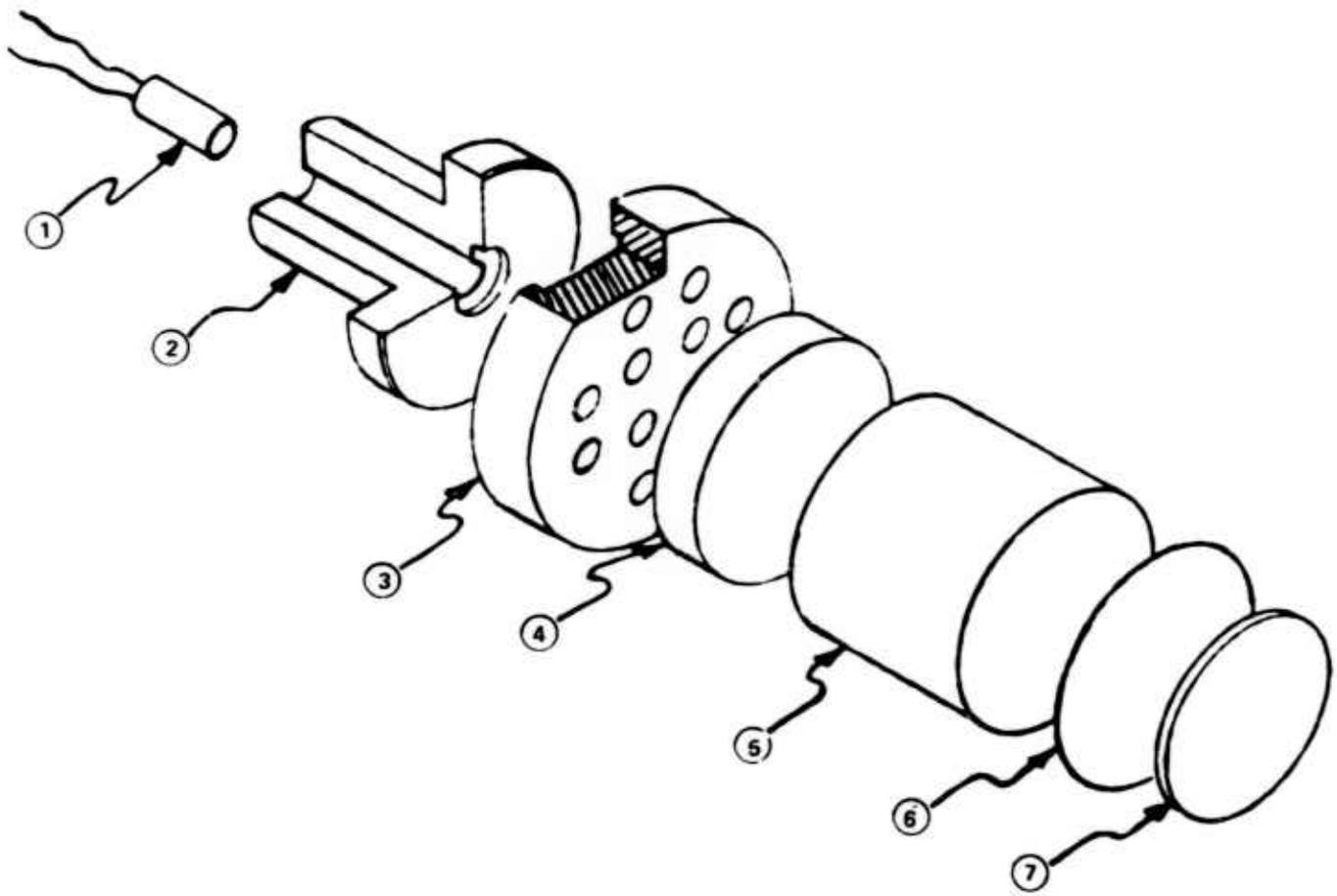

Figure 2 CALSPAN FLYER PLATE LAUNCH ASSEMBLY

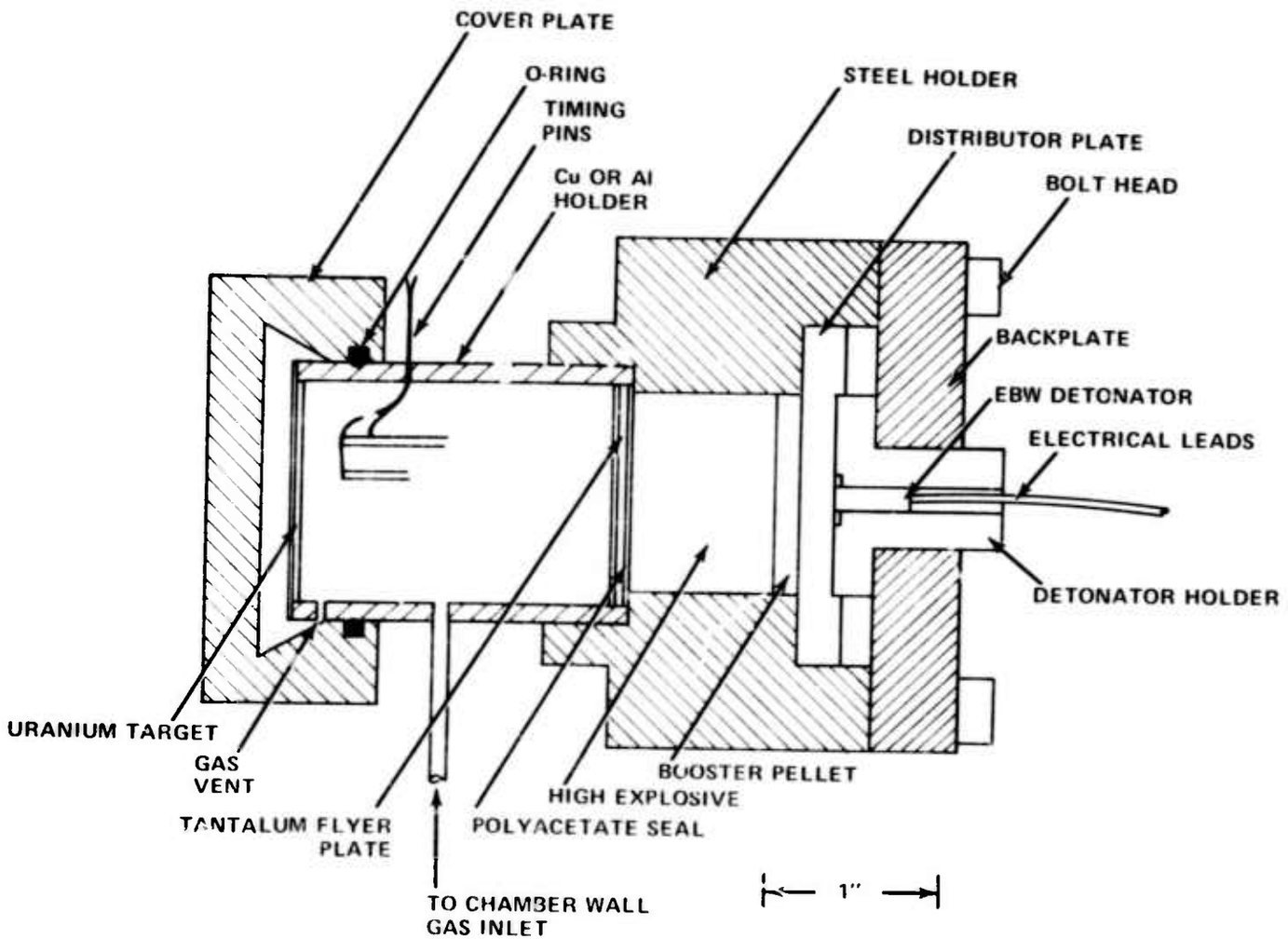

Figure 3 STEEL ENCLOSURE USED TO CONFINE DETONATION PRODUCTS AND TO PROTECT THE URANIUM TARGETS FROM EXPOSURE TO AIR

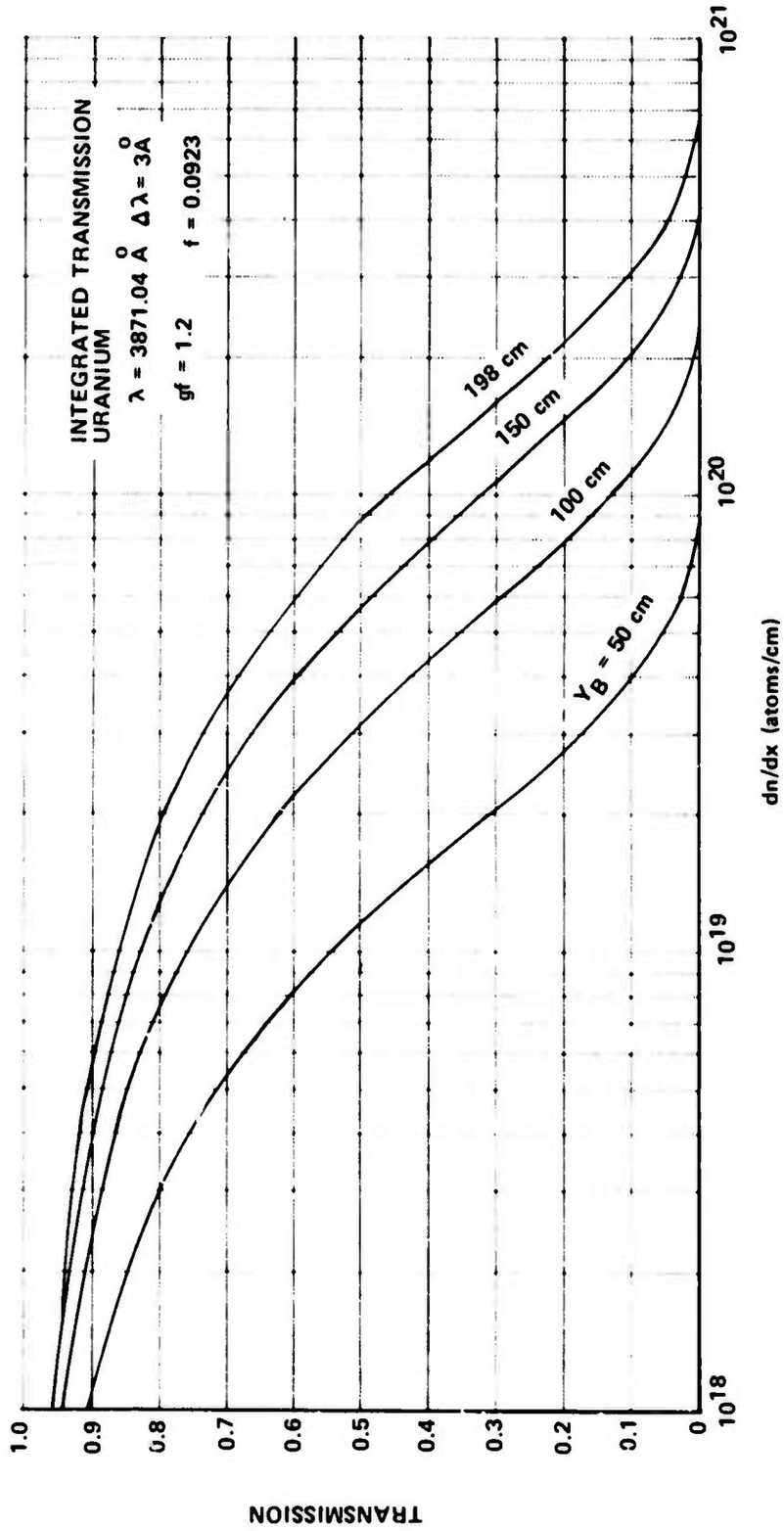

Figure 4 TRANSMISSION THROUGH URANIUM

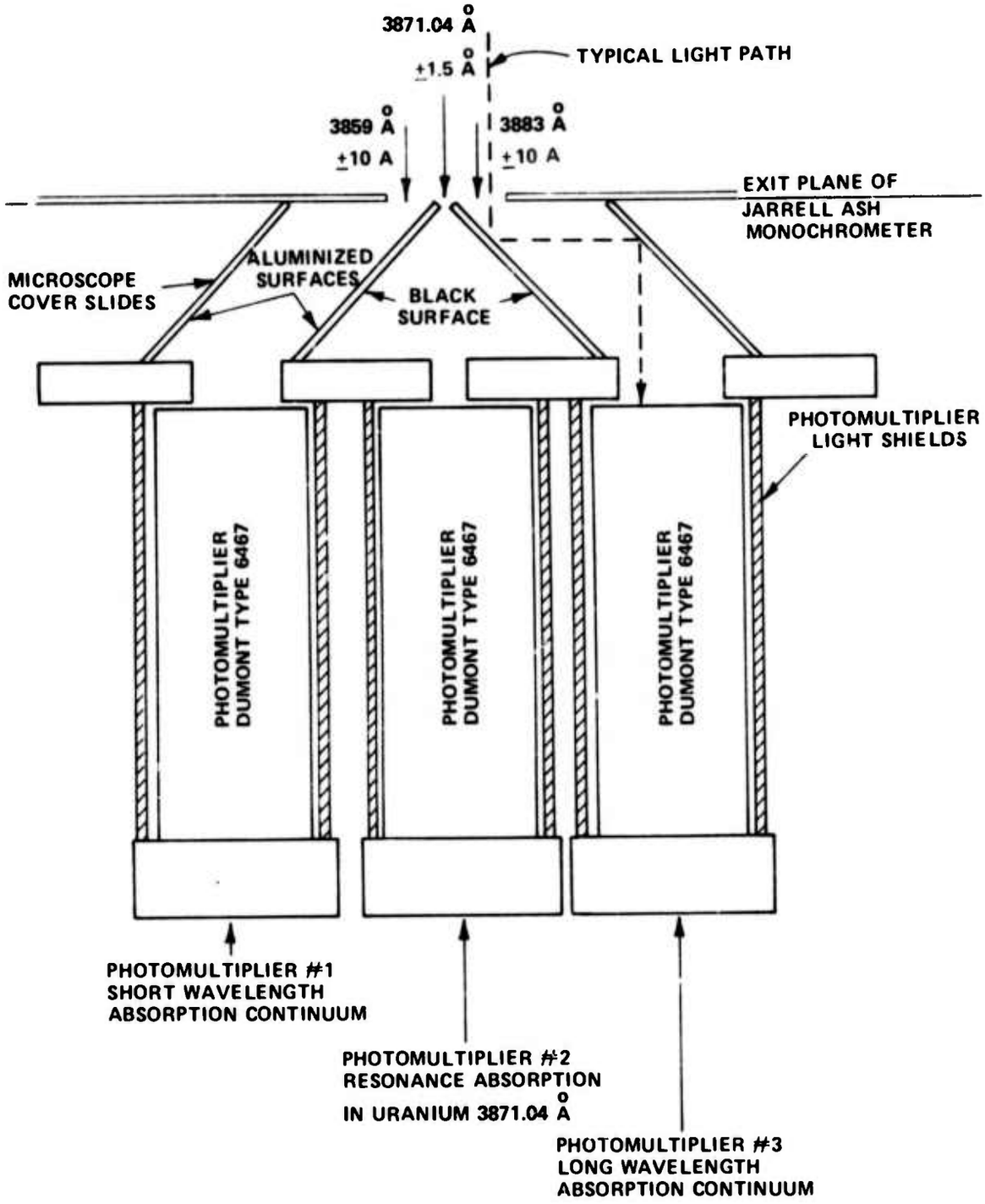

Figure 5 MONOCHROMETER EXIT-PLANE DETECTOR CONFIGURATION

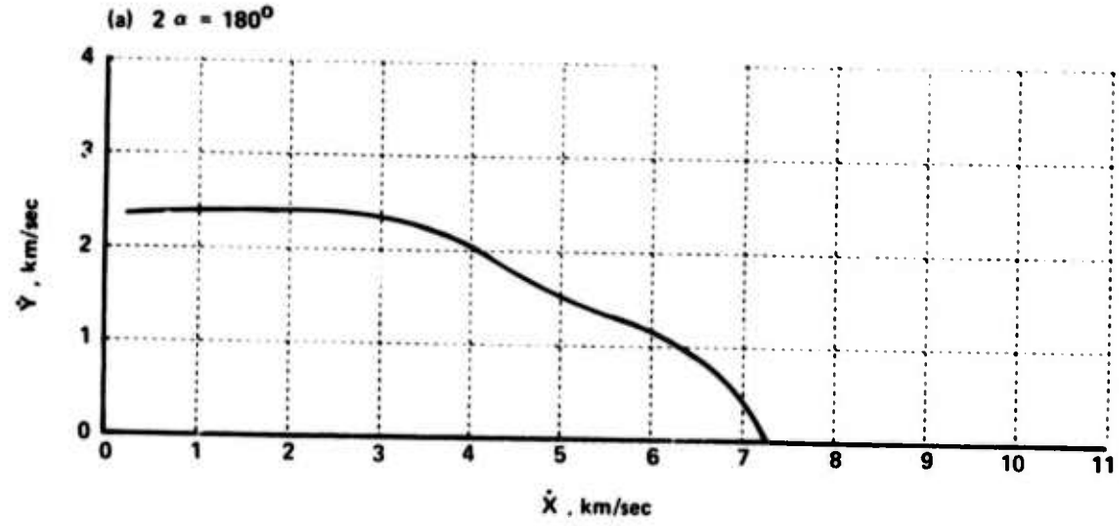

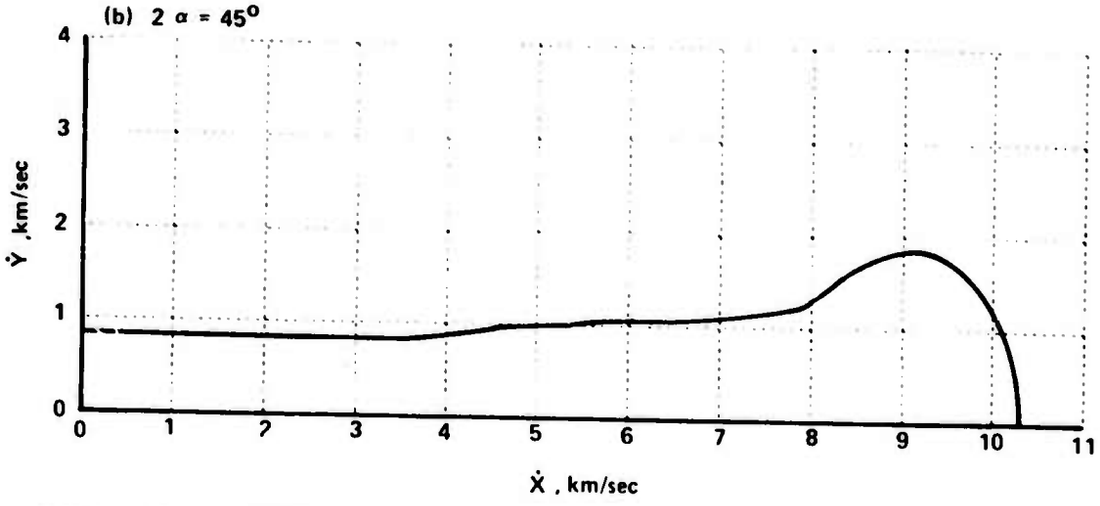

NOTE: DATA OBTAINED FROM REFERENCE 9.

Figure 6 DISTRIBUTION OF VAPOR ATOMS OVER FORWARD VELOCITY, $\dot{X}$, AND RADIAL COMPONENT, $\dot{Y}$, AS MEASURED AT THE MAX-PLANCK-INSTITUT α IS THE ANGLE OF THE H.E. CHARGE OUTPUT FACE WITH RESPECT TO THE CHARGE AXIS OF REVOLUTION

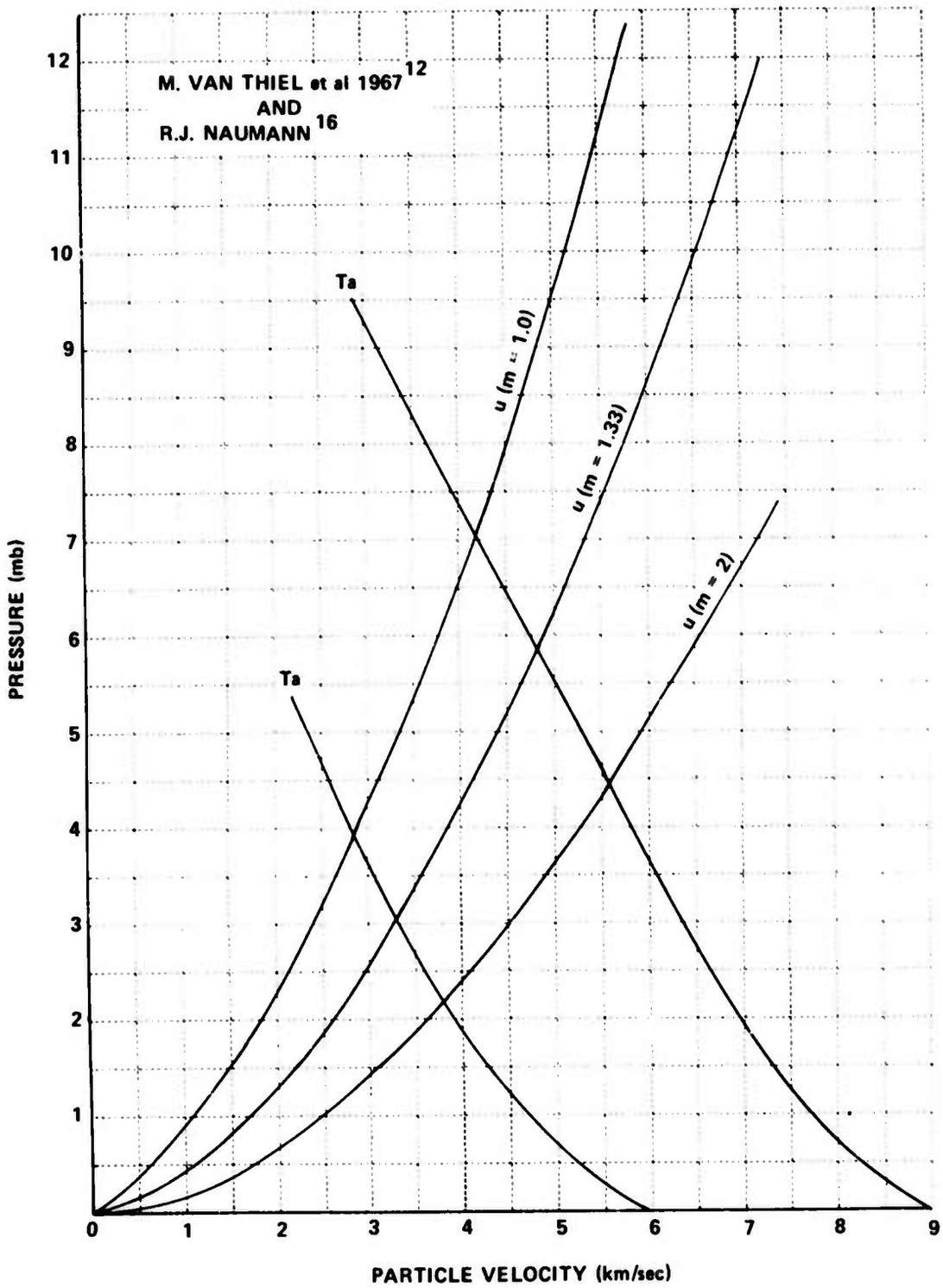

Figure 7 IMPEDANCE MATCHING FOR Ta FLYER ON URANIUM TARGETS

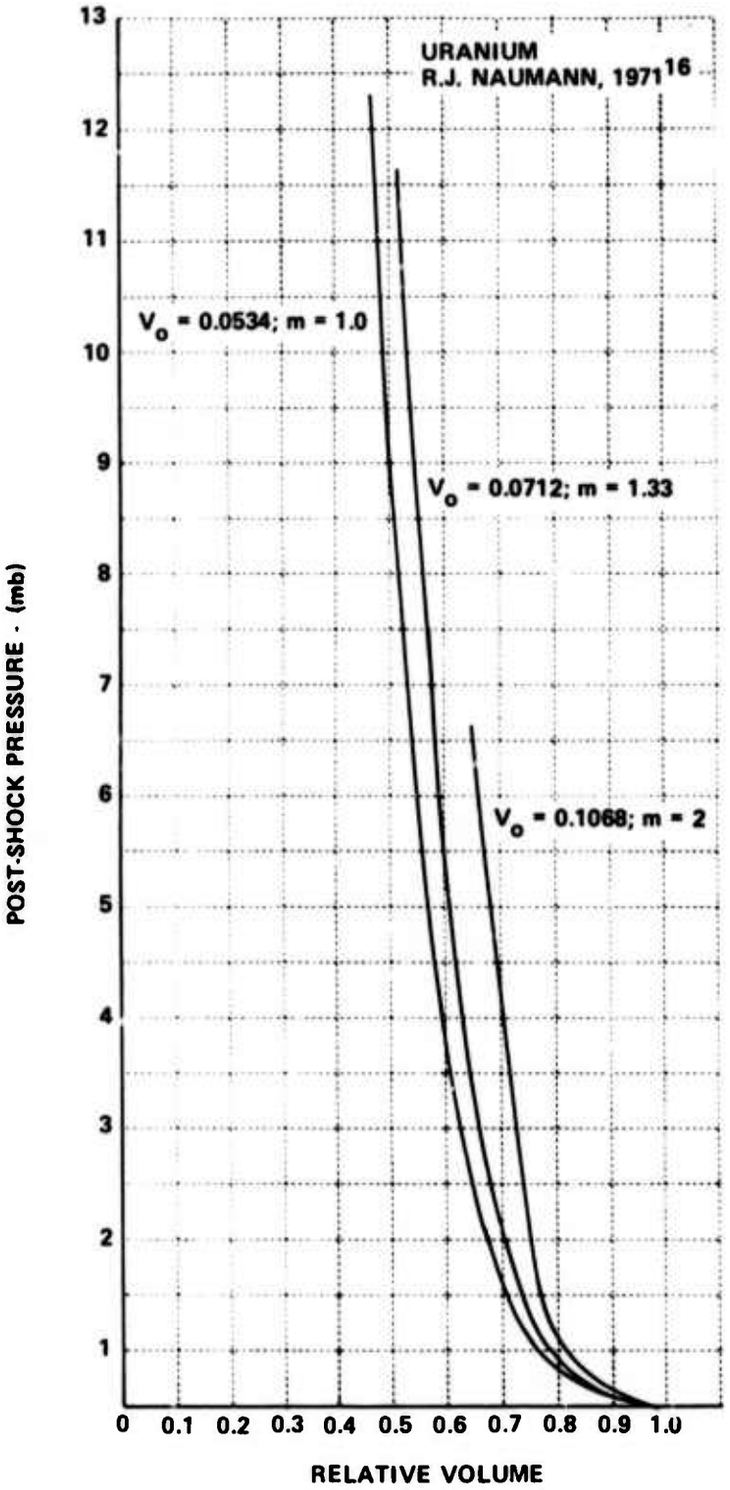

Figure 8 P-V DIAGRAM FOR URANIUM

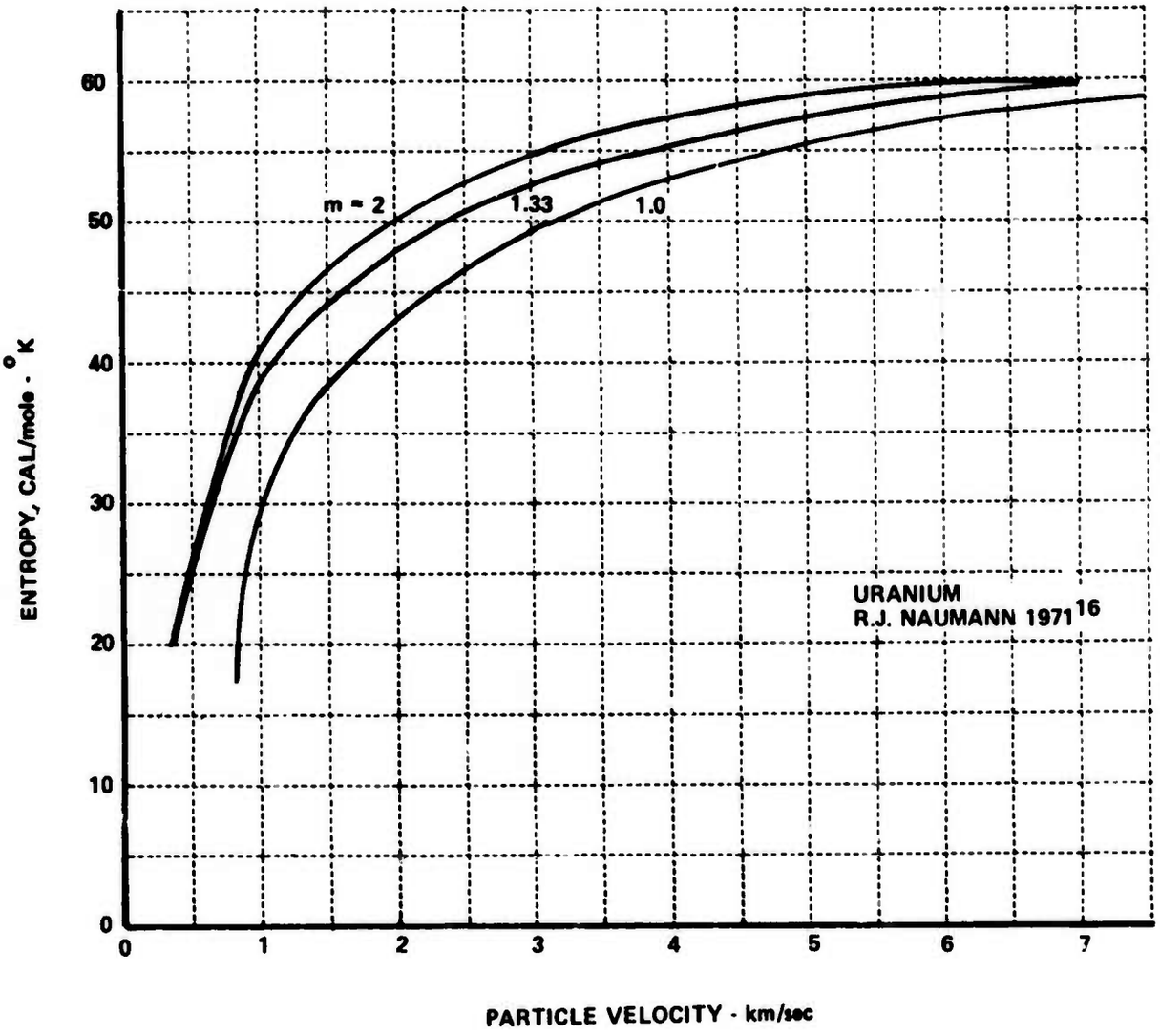

Figure 9 ENTROPY OF POROUS URANIUM AS A FUNCTION OF PARTICLE VELOCITY

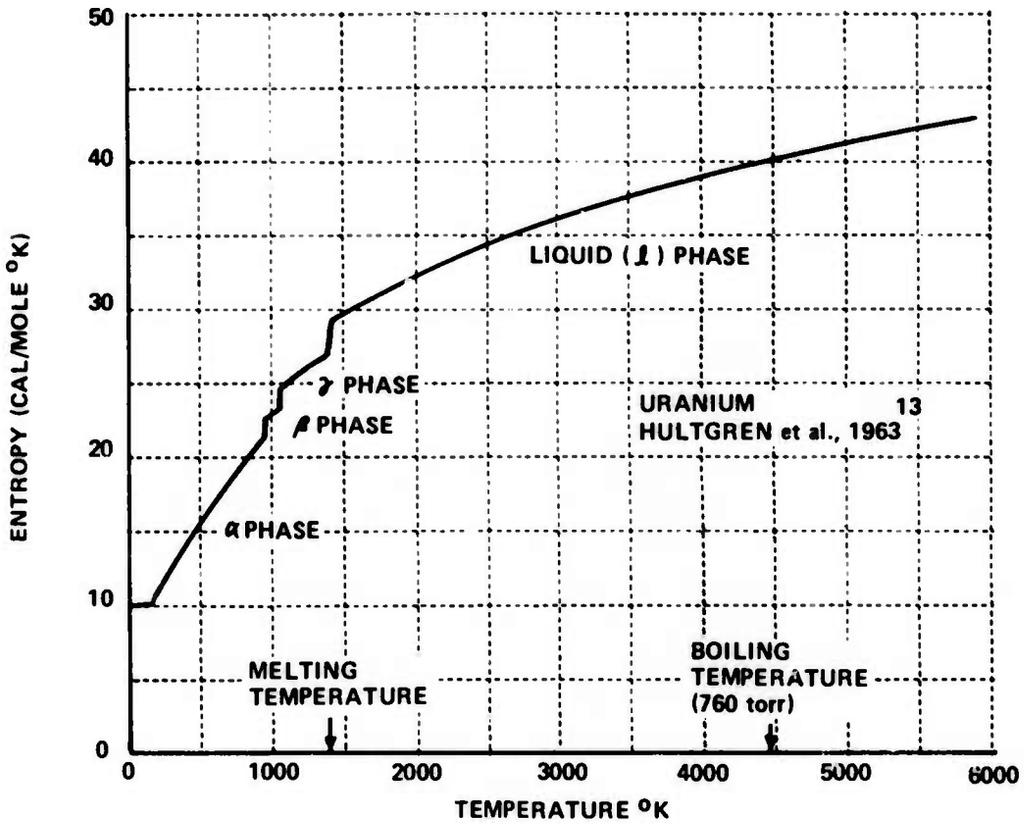

Figure 10 ENTROPY AS A FUNCTION OF TEMPERATURE FOR NORMAL CRYSTALLINE, LIQUID URANIUM

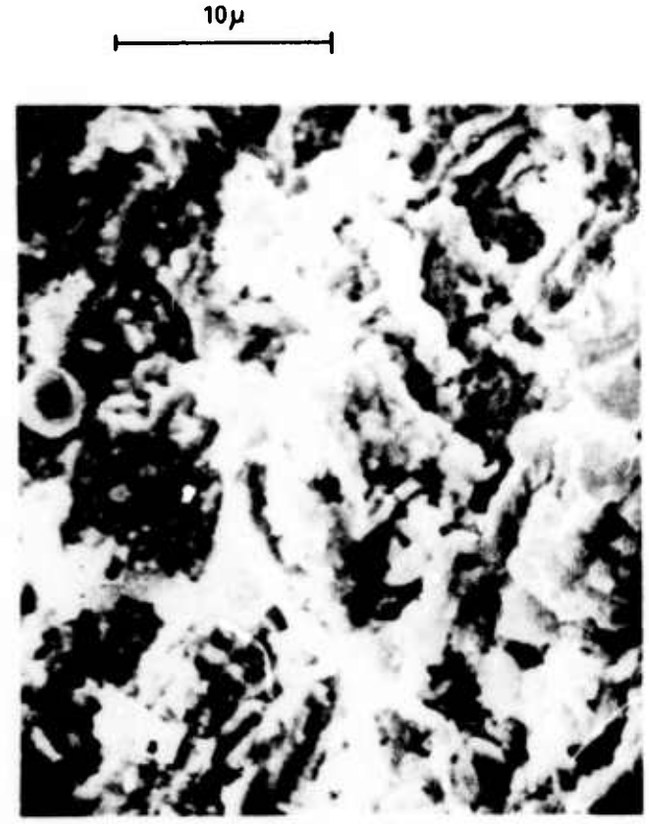

Figure 11 POROUS URANIUM SPECIMEN 70% NORMAL DENSITY, S.E.M. DIAGNOSTIC

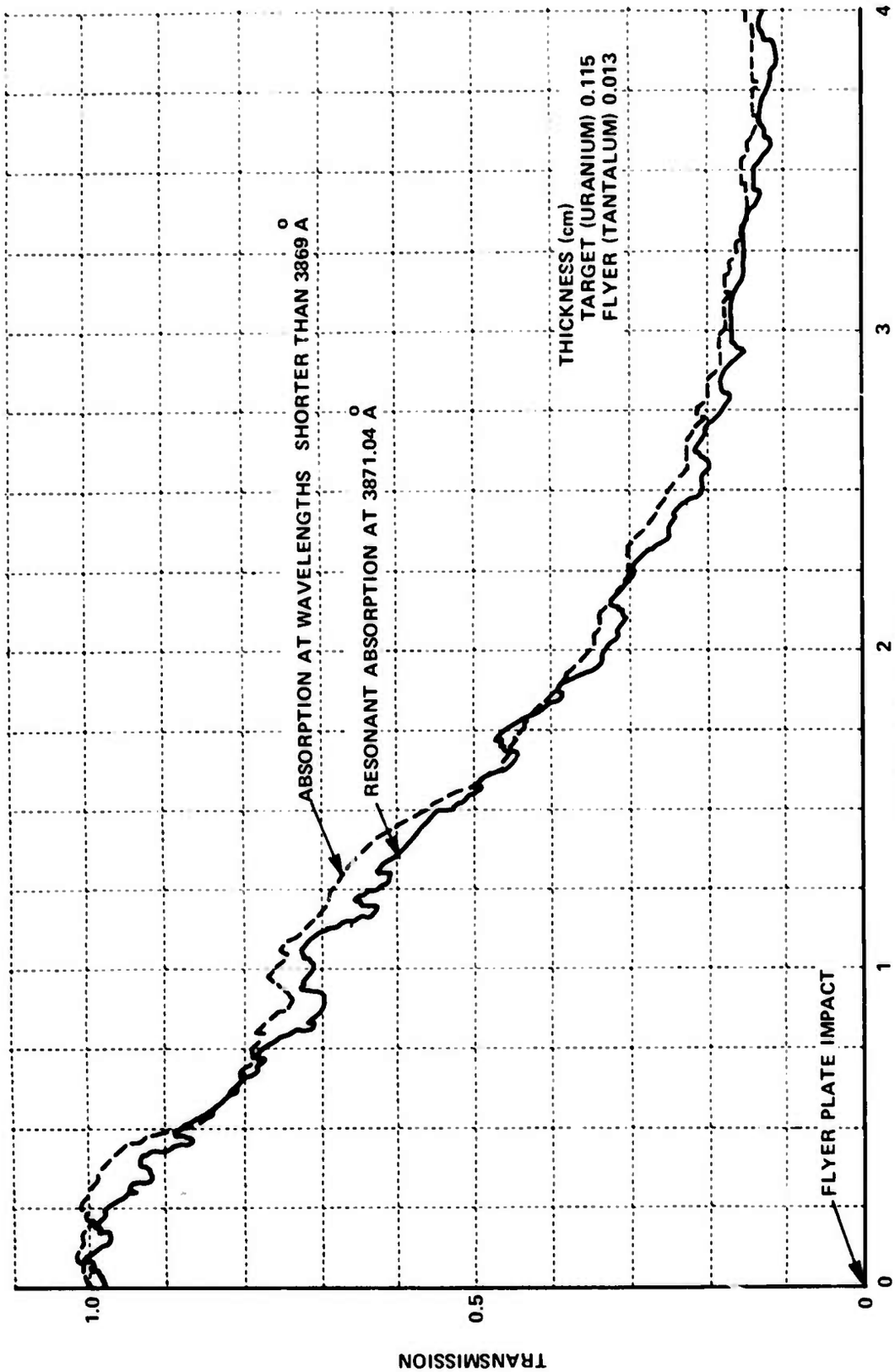

Figure 12 MONOCHROMETER SIGNAL SHOWING RESONANT ABSORPTION IN THE URANIUM SYSTEM AS A FUNCTION OF TIME AFTER TARGET SHOCK HEATING

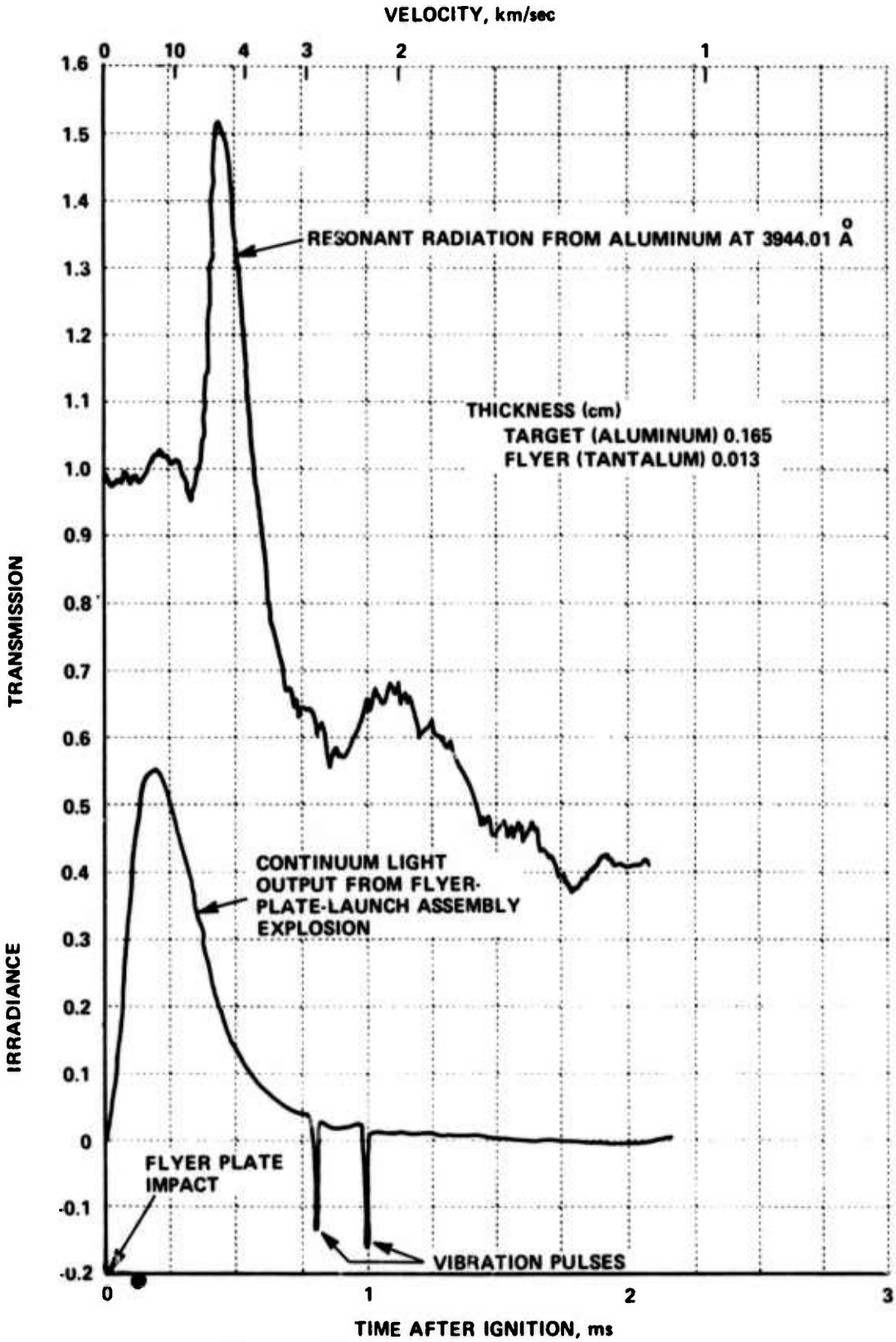

Figure 13 MONOCHROMETER SIGNAL SHOWING RADIATION IN THE ALUMINUM SYSTEM AS A FUNCTION OF TIME AFTER TARGET RELEASE, BROAD BAND LIGHT SOURCE "ON"

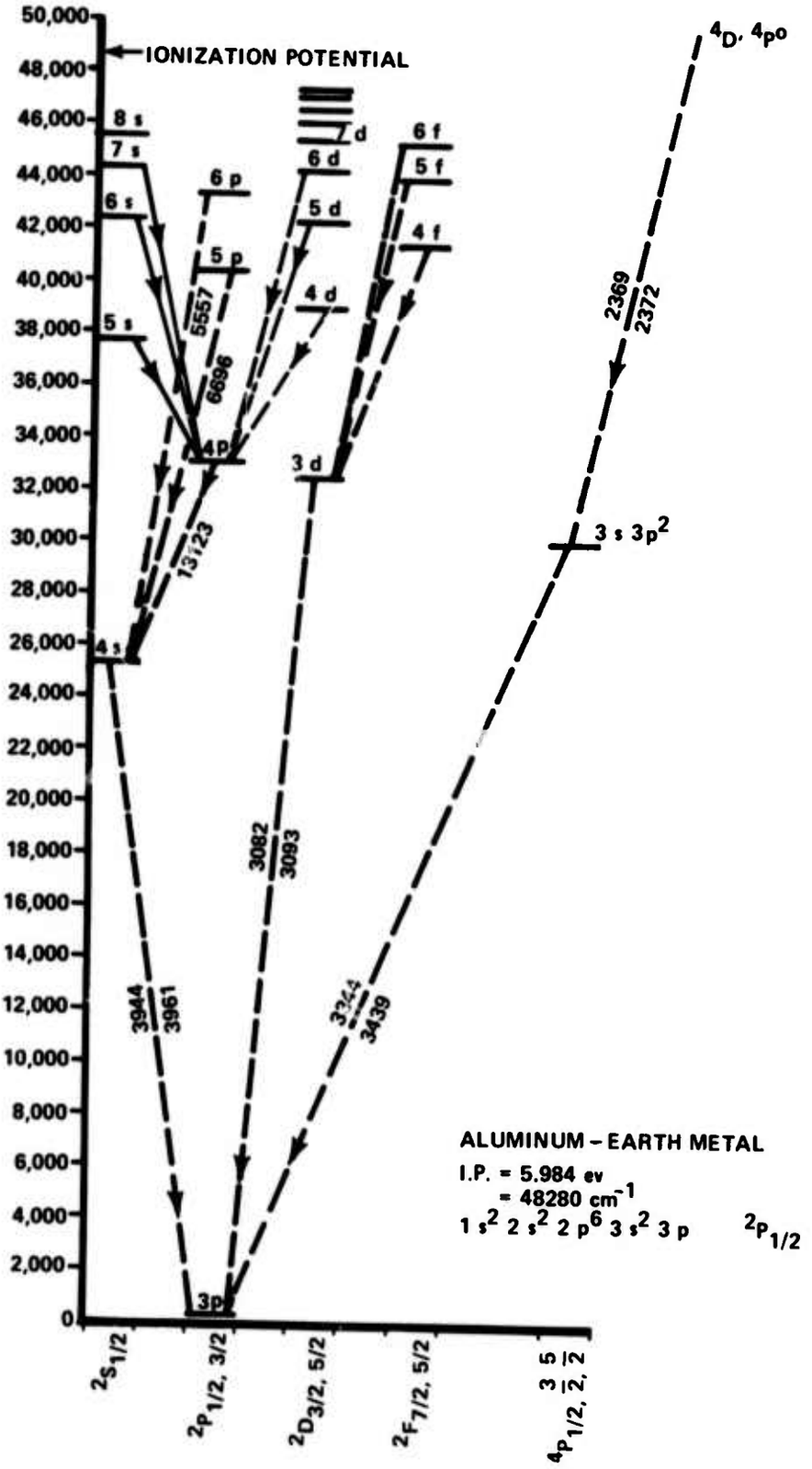

Figure 14 ENERGY LEVEL DIAGRAM OF ALUMINUM

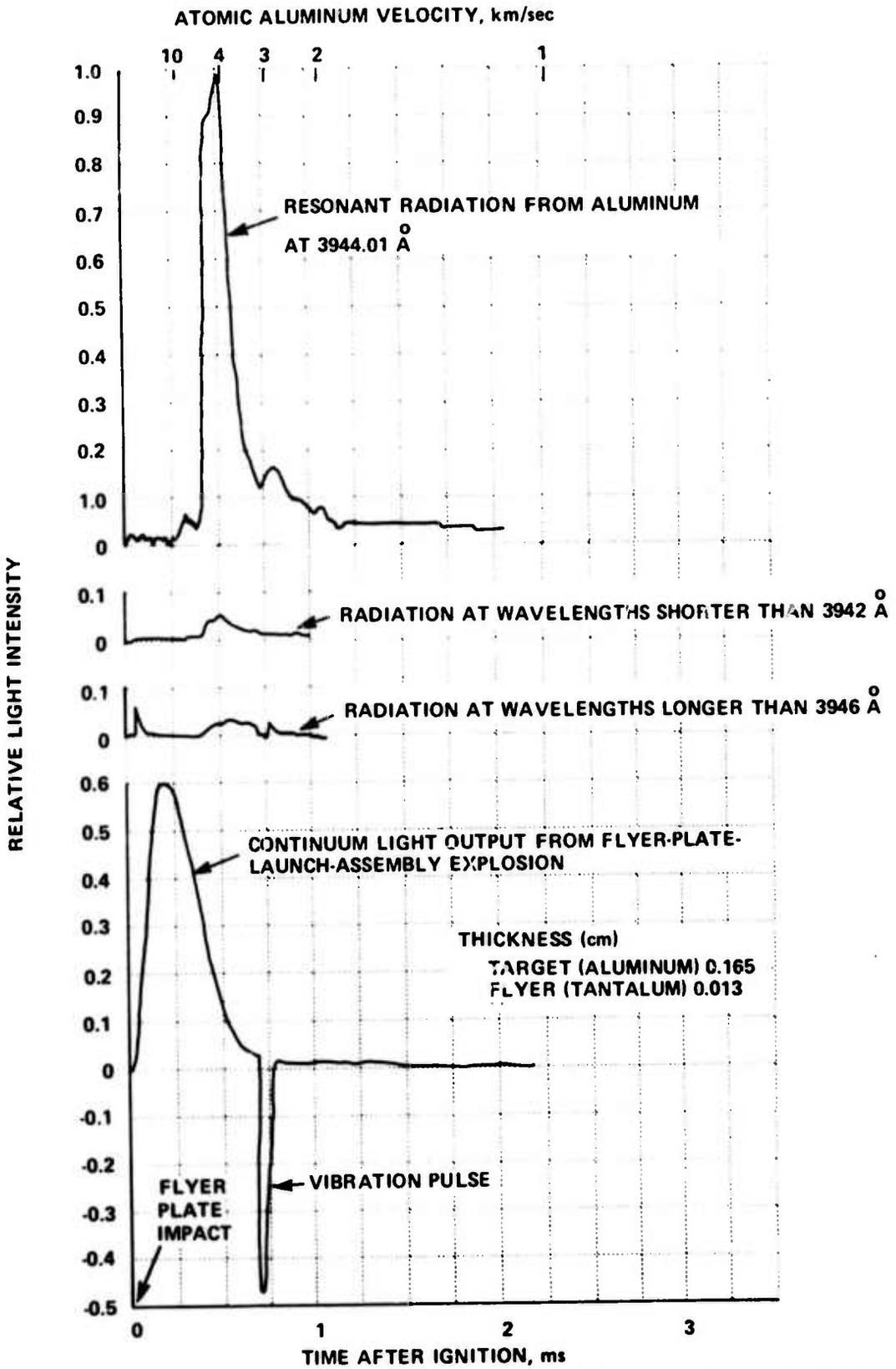

Figure 15 TIME RELATIONSHIP BETWEEN FLYER PLATE LAUNCH AND RESONANT RADIATION OBSERVED FROM ALUMINUM, CONTINUUM LAMP SOURCE "OFF"

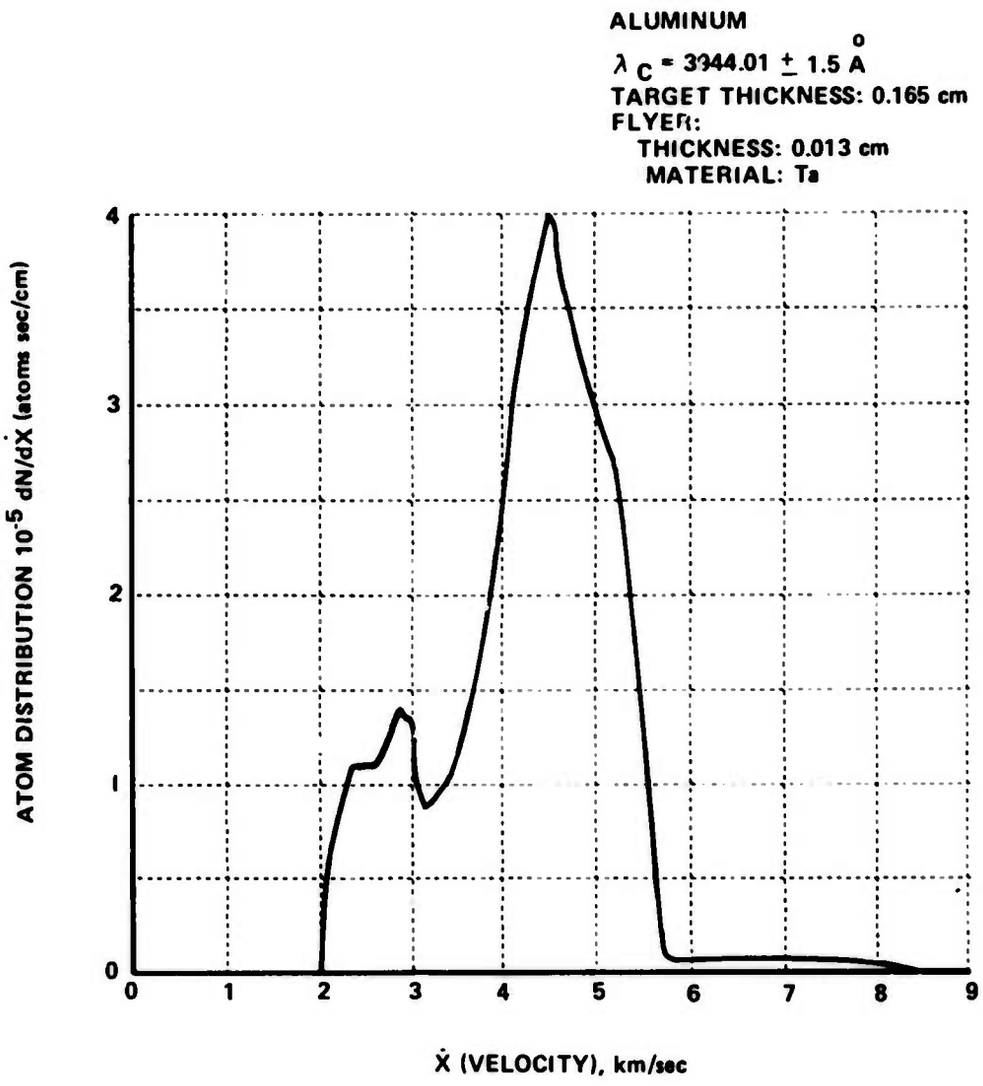

Figure 16 EXCITED ALUMINUM ATOM DISTRIBUTION OVER ITS FORWARD VELOCITY, $\dot{X}$

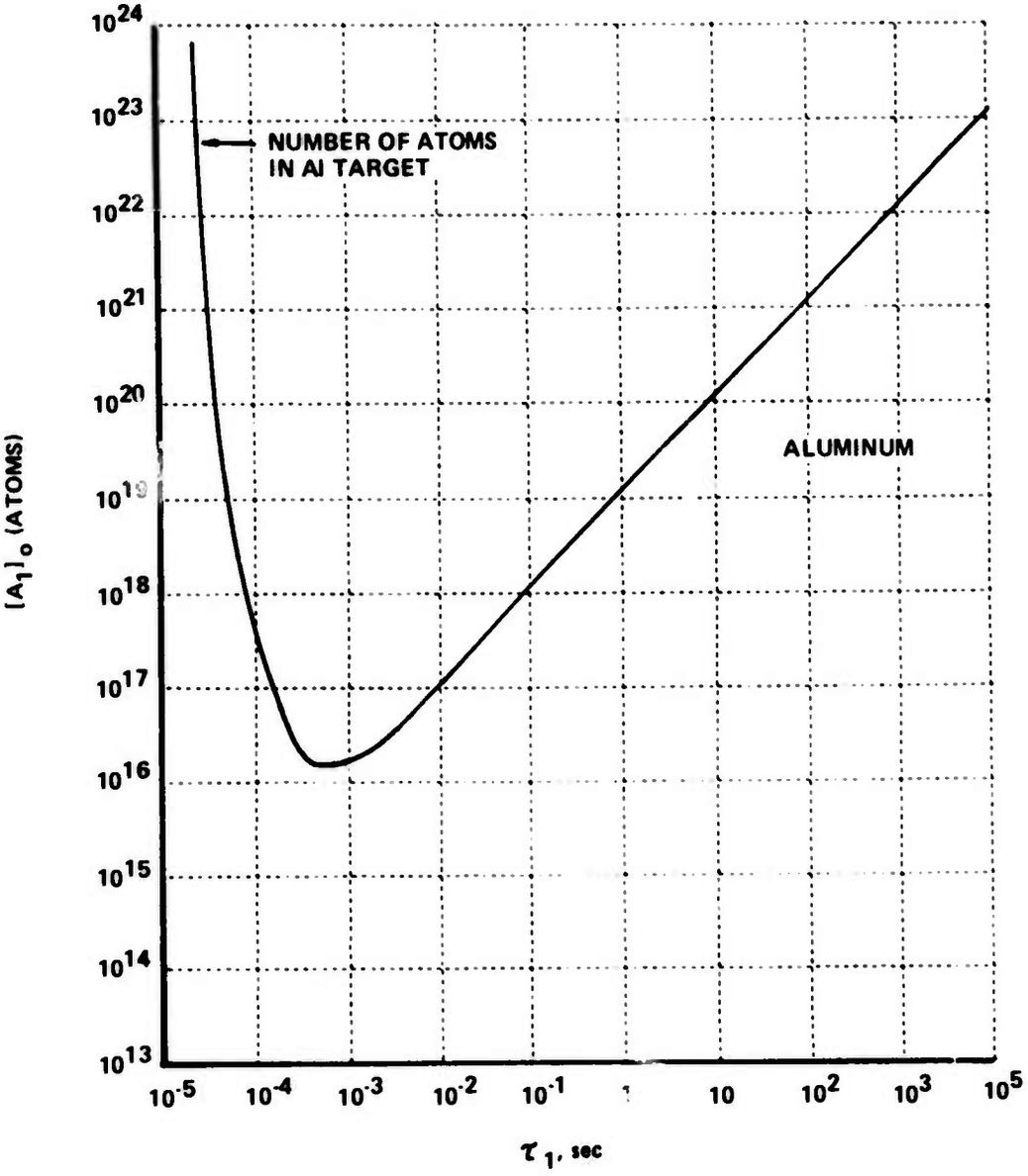

Figure 17 METASTABLE ATOM LIFETIME ESTIMATES IN ALUMINUM

APPENDIX A

FINAL REPORT

on

FABRICATION OF POROUS URANIUM DISK STRUCTURES

to

CALSPAN CORPORATION

October 1, 1973

Prime No. F30602-73-C-0157
Contract No. S-74-2

by

D. E. Lozier and W. H. Pfeifer

BATTELLE
Columbus Laboratories
505 King Avenue
Columbus, Ohio 43201

FABRICATION OF POROUS URANIUM DISK STRUCTURES

by

D. E. Lozier and W. H. Pfeifer

Objective and Approach

The objective of this program was to fabricate twenty (20) disk-shaped depleted uranium specimens 35-mm in diameter and ranging in thickness from 0.7 to 1.5 mm. Disk densities were to vary between 40 and 90 percent of theoretical density. The approach selected for fabrication consisted of preparing the uranium powder by the hydride-dehydride process, die pressing the disks, and vacuum sintering, followed by repressing to obtain the higher densities. All specimens were ground with a diamond wheel to assure the flatness and parallelism of the disk faces.

Specimen Preparation

All operations involving the preparation and pressing of the uranium powders were conducted in a vacuum-inert atmosphere dry box having a monitored dew point of $\leq$ minus 70 C and an oxygen content of approximately 10 ppm. Pressed and sintered specimens were removed from the dry box for processing such as repressing and machining by protecting them in a steel die enclosed in a sealed plastic bag or in grinding fluid.

Uranium powder having a particle size of $< 10\ \mu$ was prepared from wrought metal by subjecting the material to four successive hydride-dehydride cycles. In this process, the uranium is heated under hydrogen (> 99.999 purity) at 230 C to initiate the hydriding reaction. When the uptake of hydrogen indicates the reaction has gone to completion, the material is cooled. During the hydriding, the lattice expansion causes the uranium hydride to spall into finer particles. Subsequent reheating to 350 C under a dynamic vacuum then reduces the hydride to elemental uranium powder. Four hydride-dehydride cycles reduces the powder to $< 10\ \mu$ in particle size.

Disks of varying thicknesses were pressed in the high-purity dry box with a steel die at a pressure of 5000 psi. The disks intended for low density were then sintered for 1 hr at 800 C in a vacuum of 5×10^{-5} torr. These disks sintered to a density ranging from 44 to 50 percent of theoretical were ground to the finished dimensions as shown in Table 1. The green-pressed disks intended for the medium and higher density specimens were sintered for 1 hr at 900 C in a vacuum of 5×10^{-5} torr and repressed at 30 and 55 tsi, respectively. These disks were then ground flat and parallel to the final dimensions as shown in Table 1.

All disks were ground to final dimensions in a water-base coolant using a diamond abrasive wheel. The disks were kept immersed in the coolant at all times except at the point of wheel contact during the grinding procedure. The disks were then ultrasonically cleaned in successive baths of acetone, acetone, and 200 proof ethyl alcohol. The cleaned specimens were then covered with fresh alcohol and evaporated dry to a vacuum of 1×10^{-4} torr in the dry box airlock. The disks were weighed and measured for final density determinations within the dry box high-purity atmosphere.

Characterization

The disks were fabricated with both thickness and density as variables. The low-density disks range from 44.0 to 50.6 percent of theoretical density and the disk thickness was varied from 0.028 to 0.051 in. Disks in the medium density range are 65.0 to 72.8 percent of theoretical density and are 0.028 to 0.051 in. in thickness. The higher density disks are 83.4 to 85 percent of theoretical density and have a thickness variable of 0.029 to 0.051 in.

An optical emission spectroscopy analysis of a pressed and sintered specimen is listed below and shows the disks to be a high-purity uranium:

TABLE 1. DIMENSIONS AND DENSITIES OF DEPLETED URANIUM DISKS

Specimen Number	Diameter Average, in.	Thickness Average, in.	Volume, cc	Density, g/cc	Weight, g	Percent of Theoretical
1-L	1.3786	0.0507	1.2400	9.0322	11.2	47.41
2-L	1.3780	0.0438	1.0703	8.5022	9.1	44.63
3-L	1.3788	0.0401	0.9810	8.4607	8.3	44.41
4-L	1.3783	0.0383	0.9364	9.2909	8.7	48.77
5-L	1.3783	0.0337	0.8239	9.4671	7.8	49.69
6-L	1.3789	0.0284	0.6949	9.6416	6.7	50.61
8-L	1.3767	0.0440	1.0732	8.3861	9.0	44.02
1-M	1.3680	0.0514	1.2379	13.4905	16.7	70.81
2-M	1.3378	0.0410	1.1747	13.8758	16.3	72.83
4-M	1.3686	0.0452	1.0895	13.1252	14.3	68.89
5-M	1.3770	0.0374	0.9126	12.3822	11.3	64.99
6-M	1.3767	0.0369	0.9000	13.3333	12.0	69.99
7-M	1.3772	0.0296	0.7225	13.2871	9.6	69.74
8-M	1.3769	0.0281	0.6856	13.1271	9.0	68.90
9-M	1.3765	0.0276	0.6705	13.4228	9.0	70.46
3-H	1.3574	0.0508	1.2046	16.0219	19.3	84.10
5-H	1.3772	0.0420	1.0251	16.0959	16.5	84.49
6-H	1.3773	0.0407	0.9936	16.2037	16.1	85.05
7-H	1.3772	0.0356	0.8689	15.8821	13.8	83.37
8-H	1.3769	0.0362	0.8832	16.0778	14.2	84.39
9-H	1.3770	0.0292	0.7125	16.0000	11.4	83.98
10-H	1.3773	0.0315	0.7690	16.1248	12.4	84.64

Element	ppmw
B	2
Be	<1
Cu	15
Fe	60
Ni	5
Mn	10
Mo	3
Si	70

A metallographic examination of a disk from each of the three density groups showed the disks to be constructed from fine particles with a generally well-distributed and open porosity; however, some density variation was detected in the medium density disk examined. This specimen showed a higher density zone at the midline than on the surfaces. Figures 1, 2, and 3 are photomicrographs showing the particle structure of typical specimens in the three density groups fabricated.

Packaging

The disks were packaged for shipment within the dry box argon atmosphere. Each disk was wrapped in aluminum foil and labeled for disk identity as shown in Table 1. Disks of each of the three density groups were then sealed in separate metal containers. The containers were in turn placed in a brass cylinder with an "O"-ring sealed top fitted with a valve and pressure gage. The overpressure of approximately 12 psi of argon was then forced into the container as assurance of the atmosphere purity around the disks.

DEL:WHP/rd
October 1, 1973

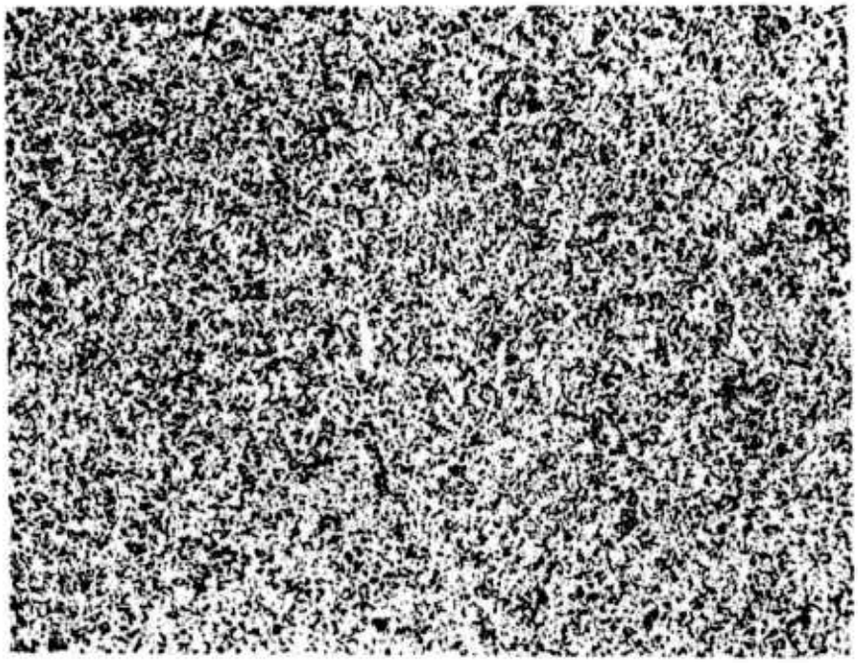

75X 7G885

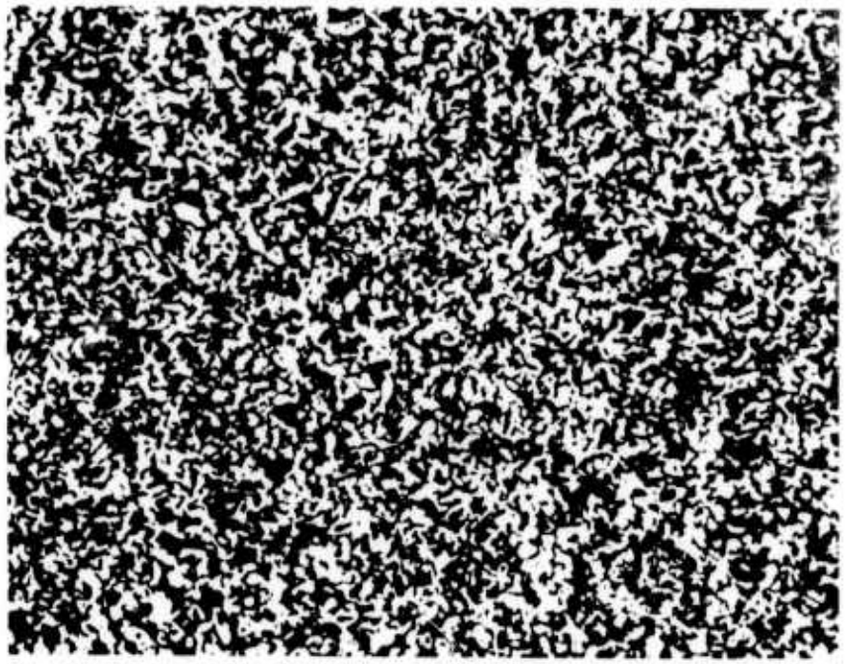

250X 7G886

FIGURE 1. TYPICAL MICROSTRUCTURE OF URANIUM DISKS IN THE LOW-DENSITY GROUP

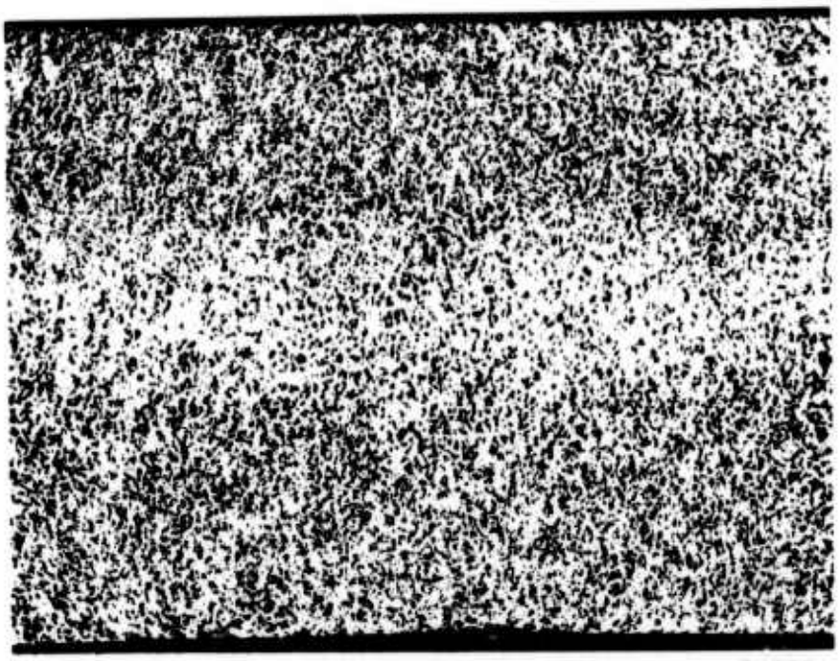

75X 7G387

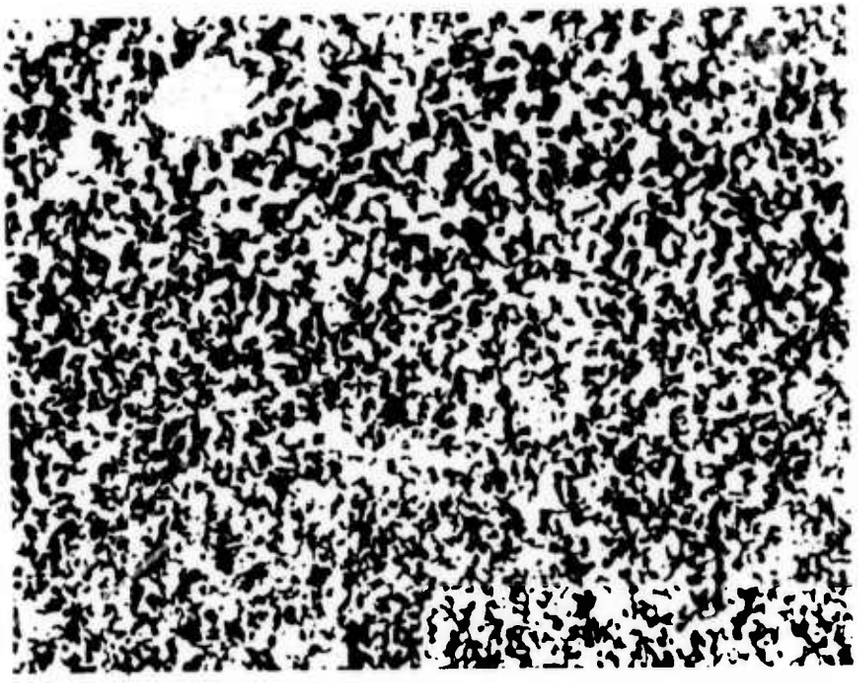

250X 7G889

FIGURE 2. TYPICAL MICROSTRUCTURE OF URANIUM DISKS IN THE MEDIUM-DENSITY GROUP

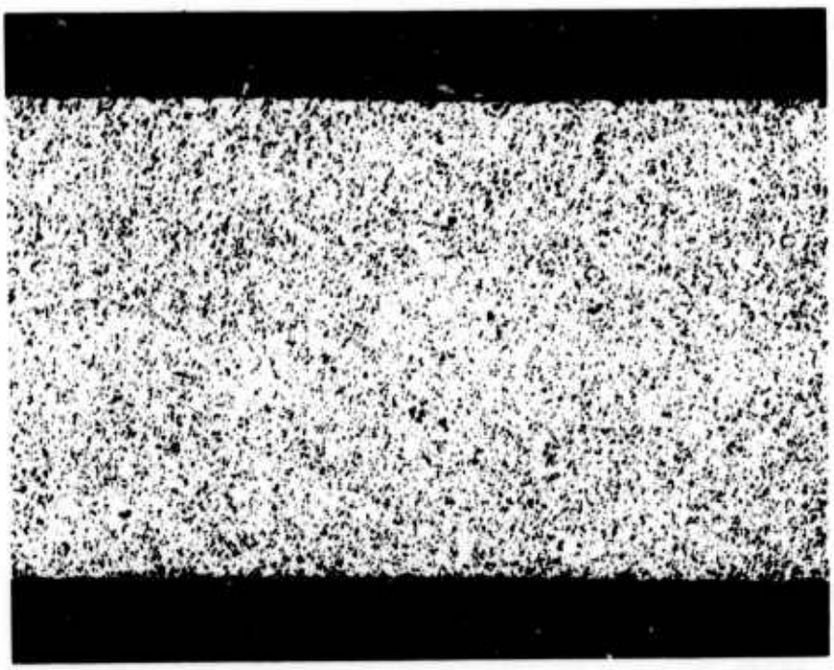

75X 7G890

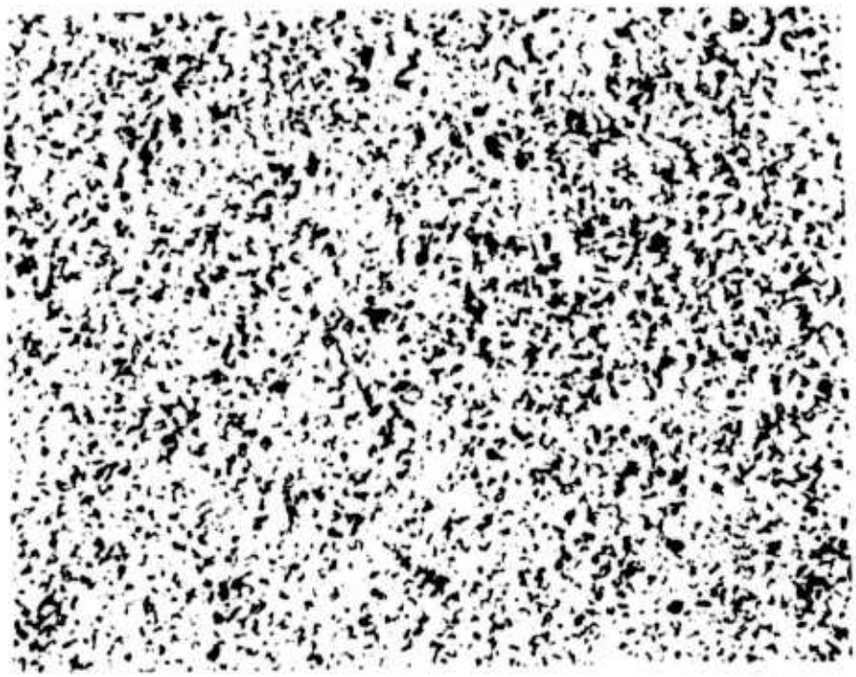

250X 7G892

FIGURE 3. TYPICAL MICROSTRUCTURE OF URANIUM DISKS IN THE HIGH-DENSITY GROUP

MISSION

OF

ROME AIR DEVELOPMENT CENTER

RADC is the principal AFSC organization charged with planning and executing the USAF exploratory and advanced development programs for electromagnetic intelligence techniques, reliability and compatibility techniques for electronic systems, electromagnetic transmission and reception, ground based surveillance, ground communications, information displays and information processing. This Center provides technical or management assistance in support of studies, analyses, development planning activities, acquisition, test, evaluation, modification, and operation of aerospace systems and related equipment.

Source AFSCR 23-50, 11 May 70